Nonlinear characteristic analysis of gear rattle based on refined dynamic model

Dong Guo
Chongqing University of Technology
Qinfeng Ning
Chongqing University of Technology
Shuaishuai Ge (gess@cqut.edu.cn)
Chongqing University of Technology https://orcid.org/0000-0001-9260-7683
Yawen Wang
The University of Texas at Arlington
Yi Zhou
Chongqing University of Technology
Yi Zhou
Chongqing University College of Mechanical Engineering
Xiaohui Shi
Chongqing University of Technology

Research Article

Keywords: Gear rattle, Bifurcation, Chaos, Lubrication effect, Drag torque, Experiment

Posted Date: March 28th, 2022

DOI: https://doi.org/10.21203/rs.3.rs-1429523/v1

Nonlinear characteristic analysis of gear rattle based on refined dynamic model

Dong Guo[a], Qinfeng Ning[a], Shuaishuai Ge[a], Yawen Wang[c], Yi Zhou[a], Yi Zhou[b], Xiaohui Shi[a]

[a] *Key Laboratory of Advanced Manufacturing Technology for Automobile Parts, Ministry of Education, Chongqing University of Technology, Chongqing, 400054, China*

[b] *College of Mechanical Engineering, Chongqing University, Chongqing, 400044, China*

[c] *Department of Mechanical and Aerospace Engineering, The University of Texas at Arlington, Arlington, TX, 76019, USA*

*Corresponding Author / Reprint Info:

Shuaishuai Ge

Email: gess@cqut.edu.cn

ABSTRACT

In order to explore the vibration response and the nonlinear behavior of gear rattle, a nonlinear dynamic model is developed in this paper considering the nonlinear oil film force, time-varying meshing stiffness, dragging torque and friction and gear backlash with time-varying characteristics. The time-varying meshing stiffness is calculated using the potential energy method. Considering the convolution and extrusion of the lubricant between the teeth, it is modeled as a nonlinear spring-damped element and a nonlinear oil film force is introduced. The drag torque is calculated numerically using fluid dynamics theory, friction principle, momentum conservation principle and Bernoulli's principle. The model is verified by comparing the bench test results with the simulation results, and the parametric study is performed to investigate the nonlinear system characteristics by means of Fast Fourier Transform, Poincare map and bifurcation diagram. The results show that as the excitation frequency increases, the system enters chaotic state under multiple frequency jumps. Excessive torque fluctuation may lead to severe rattling phenomenon of the gear pair, and making the system enter a chaotic state; As the lubricant viscosity increases, the system shows periodic, bifurcation and chaotic behavior alternately, and when the viscosity is large enough, the high frequency shock intensity decays more rapidly due to large drag torque, which is beneficial to reduce the percussion strength and prevent the system into chaos.

Keywords: Gear rattle; Bifurcation; Chaos; Lubrication effect; Drag torque; Experiment

1. INTRODUCTION

Gear rattle is a shock phenomenon that occurs in idling gear pairs and is a common problem for manual transmission gearbox. The engine torque and speed with periodic fluctuations are transmitted to transmission gears through the clutch, resulting in irregular back and forth shocks in the no-load or light-load gear pairs within the permissible working clearance The vibration causes rattling noise and annoyance to the driver and passengers.

In recent years, gear rattle has drawn increasing attention from many researchers, and much research has been carried out. For example, Karagiannis et al. [1] built a single pair of gear rattle vibration test rig and measured the displacement and velocity of gear rattle vibration to study the periodic and chaotic response of gear rattle vibration. Wang et al. [2] developed a linear dynamic model as well as a nonlinear subsystem model considering gear backlash and clutch multistage stiffness to study the system torsional vibration and gear rattle, respectively. Bozca et al. [3] studied the influence of module, number of teeth, axial clearance and backlash on gear rattle, in order to minimize rattle noise. Farshidianfar [4] developed a generalized nonlinear time-varying dynamic model of a spur gear pair and investigated the transition process from global homogeneous bifurcation to chaos in nonlinear gear systems using Melnikov analysis. Ling et al. [5] developed a six-degree-of-freedom nonlinear dynamic model using the periodic expansion method to obtain the periodic and chaotic response of the system by observing its dynamic trajectory. Yi et al. [6] proposed a nonlinear dynamic model for spur gears considering the effects of pressure angle, time-varying characteristics of gear backlash, unbalanced mass and internal and external excitation, and studied the influence of these parameters on the nonlinear behavior and the impact state.

Most of the above models consider the factors such as meshing stiffness, gear backlash, resistance torque, etc. However, the models developed assume that the gears are in a dry friction state and the lubricant is always present in the meshing gears, even if the two solid surfaces are not in contact, the reaction force between the teeth will be generated due to the squeezed oil film effect, thus ignoring the effect of the non-linear oil film force generated by the inter-tooth lubrication effect on the gear system response. In the study of gear lubrication effects, Brancati et al. [7,8] proposed an analytical model that accounts for the oil squeeze effect between the impacting teeth of mating gears. The influence of the oil-damping effects on the automotive rattling phenomenon. Theodossiades et al. [9] considered the gear impact surface as a lubricated connection and studied the effect of lubrication on light load idling gear vibration. It was shown that lubricant viscosity in the right range allows smoother transmission of motion between gears. It was shown that lubricant viscosity in the right range allows smoother transmission of motion between gears. Cruz et al. [10] considered the effect of coiling and squeezing of lubricant between teeth and showed that the oil film force is related to the viscosity of the lubricant, the entrainment speed and the speed of the squeezed oil film between the teeth of the wheel. Liu et al. [11] described the damping and stiffness of inter-tooth lubricant during gear rattle by numerical calculations.

It is well known that gear meshing excitation is very important to the dynamic performance of gears, on the base of consideration of oil film forces, it has been argued that the magnitude and direction of tooth friction force will change periodically during gear mesh, thus becomes a non-harmonic type of internal excitation and couples with other nonlinear factors such as gear backlash and time-varying stiffness, which makes the gear train exhibit complex nonlinear vibration characteristics. For example, Vaishya et al. [12,13] developed a direct contact model for Coulomb friction between gear teeth and investigated the dynamic effects caused by friction through linear

and nonlinear time-varying systems and showed that friction can reduce large oscillations under certain resonance conditions. Chone [14] constructed a direct contact elastic deformation model considering friction and analyzed the effect of friction on the gear vibration response. The results show that the effect of friction on the non-linear behavior of gears is small and has a positive effect, but the scholar modelled the friction coefficient as a constant and did not consider the time-varying characteristics of the friction coefficient. In the case of gear backlash studies, most of the existing gear backlash models only consider compensation errors and only consider as a constant backlash function. In fact, the backlash of gear teeth changes during the motion due to wear of gear teeth and deformation of support bearings and shafts. The study of the nonlinear dynamic characteristics of dynamic backlash gear systems has a wide range of applications. For example, Li et al. [15] considered that the presence of lubricant changes the relative displacement of gears and investigated the effect of gear backlash on the dynamic behavior of gears by developing a non-linear mathematical model of gear backlash. In the study of resistive torques, numerous scholars have proposed different calculation models from different perspectives. For example, Lauster [16] fitted an expression for the churning torque to a churning loss test on a commercial vehicle transmission. Changenet [17] used a single pair of spur gears as the test object and carried out extensive tests considering gear parameters, lubricant oil parameters and operating parameters to fit a new formula for calculating the churning torque. Gorla et al. [18] used a CFD method to investigate the churning power loss for different parameters at high-speed conditions and verified it experimentally. However, most of the existing calculation methods are based on semi-empirical formulas obtained through experimental fitting and have a limited scope of application. The CFD-based simulation usually used simplified mesh, which will lead to reduced efficiency and accuracy. There is still a lack of a general and effective theoretical model for calculating the churning resistance torque.

Based on the summary of the above references, although some dynamic models exist to investigate the non-linear characteristics of gears, most do not take into account the comprehensive effect of influencing parameters, such as drag torque, non-linear oil film force, lubricant viscosity, time-varying meshing stiffness, friction force and gear backlash. Therefore, this paper aims at establishing a non-linear dynamic model of gear rattling that considers the combined effect of above-mentioned parameters, and investigating the non-linear behavior and severity of gear rattling. The rest of the paper is structured as follows. Section 2 introduces the gear dynamic model which includes the calculation of time-varying mesh stiffness and dragging torque. The influence of time-varying friction coefficient on the dynamical behavior is also discussed. Section 3 presents the experimental validation. Section 4 presents the parametric analysis for various parameters. The final conclusions are given in Section 5.

2. DYNAMIC MODELLING OF GEAR SYSTEM

2.1. Gear dynamic model

In order to accurately explore the nonlinear dynamic characteristics of gear pair under the action of many nonlinear strong factors, taking a certain gear of a dual clutch transmission as the research object, A single degree of freedom coupled friction force model was established, which considered the nonlinear factors such as time-varying meshing stiffness, meshing damping, nonlinear backlash, time-varying friction coefficient and nonlinear oil film force, the dynamics

model is shown in Fig. 1. Here C_m and K_m represent gear meshing damping and time-varying meshing stiffness, respectively, and θ_p, θ_g represent the angular displacement of the two gears, the r_{bp} and r_{bg} represent the base circle radius of the main and driven gears, respectively.

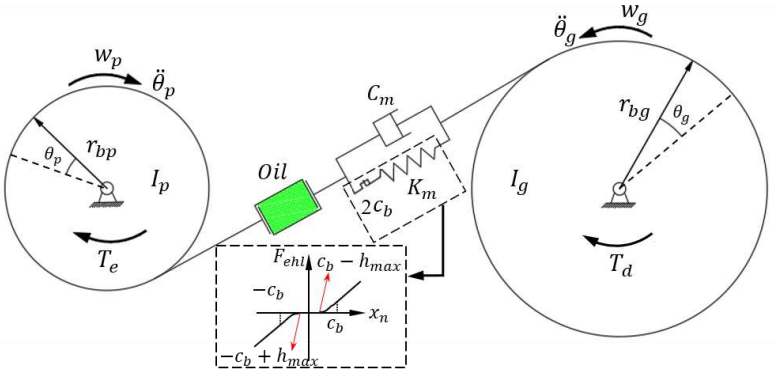

Fig. 1. Meshing dynamics model of gear pair.

According to Newton's second law, the force analysis of the gear system is carried out, and the mathematical model is shown in Eq. (1)-(3):

$$T_e - T_{meshp} = I_p\ddot{\theta}_p \tag{1}$$

$$T_{meshg} - T_d = I_g\ddot{\theta}_g \tag{2}$$

$$T_{mesh\,(i)} = \begin{cases} F_{ehl} r_{b\,(i)} \cos\beta_b - T_{ef(i)} & |x_n| \geq c_b \\ F_{hdl} r_{b\,(i)} \cos\beta_b - T_{hf(i)} & |x_n| < c_b \end{cases} \quad i = p \ , \ g \tag{3}$$

$$x_n = (r_p\theta_p - r_g\theta_g)/\cos\alpha_n \cos\beta \tag{4}$$

where x_n is the normal relative displacement of helical gear; $r_{b(i)}$ represent the radius of the base circle of the gear, Angle markers p and g respectively represent the active and driven gear; $T_{mesh(i)}$ is the torque produced by meshing force F_{mesh} and friction force F_f during tooth meshing; F_{ehl} represents the meshing force when the gear is in direct contact, F_{hdl} represents tooth surface fluid lubrication force; $T_{ef(i)}$ and $T_{hf(i)}$ represent the friction torques under two contact states, respectively; β_b is spiral Angle of gear base circle, I_p and I_g represent the rotational inertia of the main and driven gears, respectively; $\ddot{\theta}_p$ and $\ddot{\theta}_g$ represent the angular acceleration of the two gears, respectively; T_e and T_d represent driving torque and towing torque, respectively; The driving torque T_e can be expressed as:

$$T_e(t) = T_m + T_A \sin(2\pi f_m t) \tag{5}$$

where T_m represents the mean torque of driving torque, T_A represents the amplitude of torque fluctuation, f_m is the excitation frequency, $f_m = n_p/60$, n_p is the driving gear speed.

2.2. Gear contact model

The model established in this paper is a dynamic model with lubrication effect considered. Therefore, the gear meshing force F_{mesh} in lubrication state includes two aspects: That is, the dynamic meshing force F_{ehl} generated by direct contact of gear teeth and the fluid lubrication force

generated by extrusion and suction of lubricating oil when the tooth surfaces do not contact. At this point, the lubricating oil film between teeth is equivalent to a spring damping element and presents nonlinear oil film force F_{hdl}. The two contact forms are shown in Fig. 2.

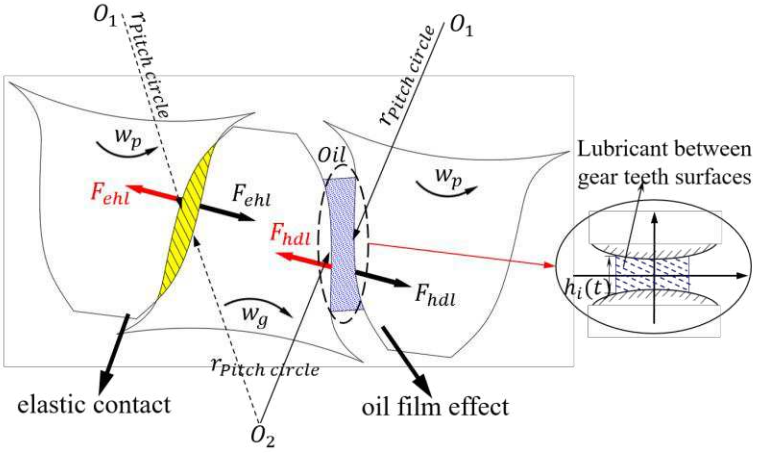

Fig. 2. Schematic diagram of gear contact form.

However, in the process of gear processing, in order to avoid thermal expansion jam, and to produce ideal lubrication, it is necessary to maintain adequate clearance. According to reference [15] backlash $2c_b$ is symmetrically distributed and lubricants exist between the two tooth surfaces and change the relative displacement of gears. Therefore, considering the backlash, the nonlinear deformation function $\epsilon(t)$ is used to modify x_n, and the piecewise function expression is shown in Eq. (6):

$$\epsilon(t) = \begin{cases} x_n - c_b & x_n > c_b - h_{max} \\ 0 & |x_n| \le c_b - h_{max} \\ x_n + c_b & x_n < -c_b + h_{max} \end{cases} \tag{6}$$

where h_{max} is the upper limit of the central oil film thickness at which the meshing force is begins, $c_b - h_{max}$ is the nonlinear backlash affected by h_{max}. The direct contact condition is regarded as a special case of lubrication condition, there is no oil between the two tooth surfaces, i.e, $h_{max} = 0$ mm.

Therefore, the meshing force F_{mesh} of gears in lubrication state can be expressed by piecewise function as shown in Eq. (7):

$$F_{mesh} = \begin{cases} F_{ehl\,1} = K_m \cdot \epsilon(t) + C_m \cdot \dot{x}_n & x_n > c_b - h_{max} \\ F_{hdl} & |x_n| \le c_b - h_{max} \\ F_{ehl\,2} = K_m \cdot \epsilon(t) + C_m \cdot \dot{x}_n & x_n < -c_b + h_{max} \end{cases} \tag{7}$$

where x_n is the normal relative displacement of helical gear, C_b is half of the backlash, θ_p and θ_g represent the angular displacement of the main and driven gears respectively, r_{bp} and r_{bg} represent the base circle radius of the main and driven gears respectively, K_m is time-varying meshing stiffness of gear, C_m is gear meshing damping [19,20] which can be expressed as:

$$C_m = 2\xi\sqrt{K_m {r_{bp}}^2 {r_{bg}}^2 I_p I_g / ({r_{bp}}^2 I_p + {r_{bg}}^2 I_g)} \tag{8}$$

where ξ represents the damping ratio coefficient, which usually ranges from 0.03 to 0.17, and the value in this paper is 0.1.

For the meshing stiffness, there are different calculation methods such as Weber's method [21], ISO standard [22], and potential energy principle [23,24,25,26] Among them, the potential energy method has better accuracy and is widely used in many references as an analytical calculation method for gear mesh stiffness, and the gear teeth are usually considered as non-uniform cantilever beams in the calculation, as shown in Fig. 3. Four kinds of stiffnesses are generated during the meshing of spur gears: Hertzian contact stiffness k_h bending stiffness k_b, shear stiffness k_s and axial compression stiffness k_a. The potential energy method solves them jointly to obtain the single-tooth time-varying meshing stiffness k of the gear, as shown in Eq. (9).

$$k = 1/(\frac{1}{k_h} + \frac{1}{k_{bp}} + \frac{1}{k_{sp}} + \frac{1}{k_{ap}} + \frac{1}{k_{fp}} + \frac{1}{k_{bg}} + \frac{1}{k_{sg}} + \frac{1}{k_{ag}} + \frac{1}{k_{fg}}) \tag{9}$$

Then, slice the helical gear and simplify it into several spur pieces of gears (as shown in Fig. 3). Finally, the time-varying meshing stiffness K_m of the helical gear was obtained considering the changes of contact degree and meshing period, which could be expressed by Fourier series as follows:

$$K_m(t) = k_0 + \sum_j^m k_{2j-1}\cos(jwt) + k_{2j}\sin(iwt) \tag{10}$$

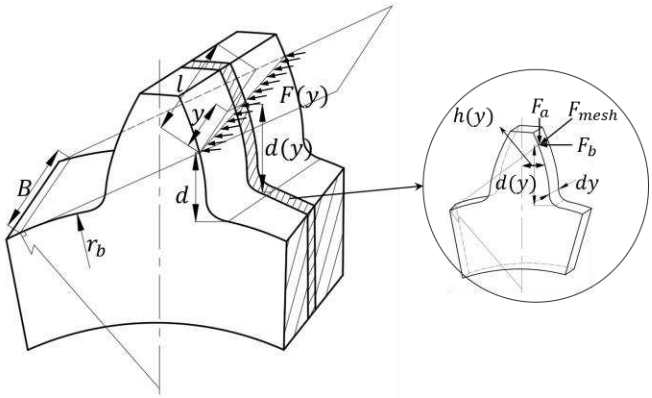

Fig. 3. Slice model of helical gear.

The time-varying meshing stiffness curve of helical gear is shown in Fig. 4, where the dotted line represents the time-varying meshing stiffness of single tooth in meshing cycle, and the solid line represents the comprehensive time-varying meshing stiffness of multiple tooth meshing.

When the tooth surfaces do not contact, the lubricating oil between the two meshing teeth can be regarded as a nonlinear elastic-damping element with time variation. Under the action of tooth surface extrusion and coiling, the fluid lubrication force is produced, which will affect the dynamic response of the gear meshing. Therefore, the nonlinear oil film force calculation model in this paper is shown in in Eq. (11)-(12):

$$F_{hdl} = \begin{cases} C^{Wedge} \cdot u - C^{Squeeze} \cdot \frac{dh_i}{dt} & \frac{dh_i}{dt} < 0 \begin{cases} h_{max} > \delta_i > h_{min} & h_i = \delta_i \\ h_{min} > \delta_i > 0 & h_i = h_{min} \end{cases} \\ C^{Wedge} \cdot u & \frac{dh_i}{dt} \geq 0 \begin{cases} h_{max} > \delta_i > h_{min} & h_i = \delta_i \\ h_{min} > \delta_i > 0 & h_i = h_{min} \end{cases} \end{cases} \tag{11}$$

$$C^{Wedge} = \frac{2L\eta_0 r_{eq}}{h_i} \quad 、 \quad C^{Squeeze} = \frac{3\pi L\eta_0}{\sqrt{2}}\left(\frac{r_{eq}}{h_i}\right)^{3/2} \tag{12}$$

where the C^{Wedge} and $C^{Squeeze}$ are equivalent damping coefficients of coiling and extrusion, respectively; L represents the meshing curve of helical gear, r_{eq} represents the equivalent radius of curvature of gear, h_i represents oil film thickness, dh_i/dt is the oil film extrusion speed, η_0 represents dynamic viscosity of lubricating oil, u is the suction speed of lubricating oil, which can be expressed as:

$$u = \left(v_p + v_g\right) cos\,\beta / cos\,\beta_b \tag{13}$$

where v_p and v_g represent the rolling speed of the tooth surface of the main and driven gears. The oil film thickness can be expressed as:

$$h_i = \begin{cases} c_b - \frac{r_p\theta_p - r_g\theta_g}{cos\,\alpha_n\,cos\,\beta} & r_p\theta_p > r_g\theta_g \\ c_b & r_p\theta_p = r_g\theta_g \\ c_b + \frac{r_p\theta_p - r_g\theta_g}{cos\,\alpha_n\,cos\,\beta} & r_p\theta_p < r_g\theta_g \end{cases} \tag{14}$$

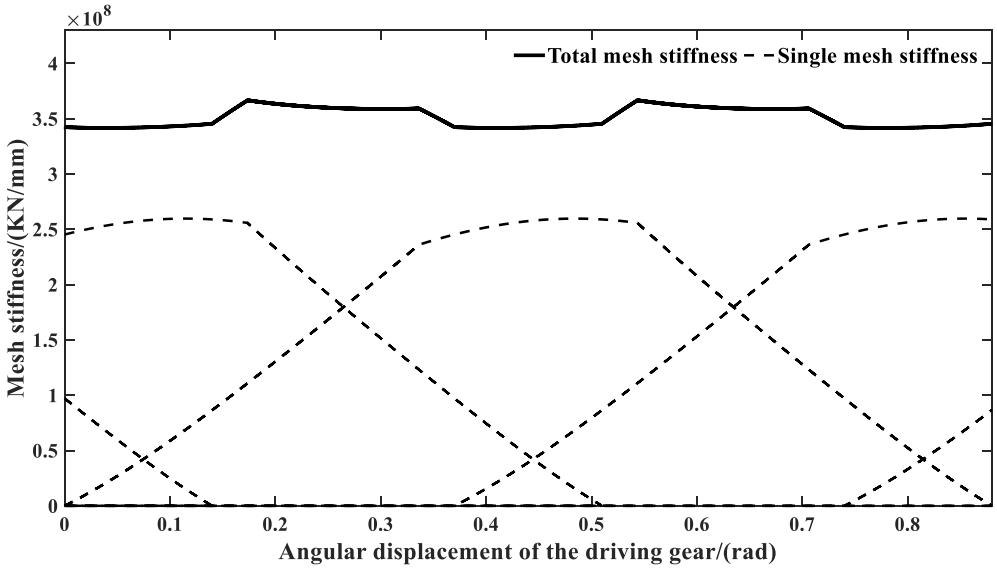

Fig. 4. Mesh stiffness of helical gear.

2.3. Drag torque

The drag torque T_D of the empty gear mainly includes three aspects: the gear oil stirring resistance torque T_g, the roller bearing torque T_{rb} and the oil film shear resistance torque T_{sy}. Since the torque of the gear power transmission is much larger than the drag torque, the bearing gear in this paper ignores the influence of the drag torque, while ignoring the main wind resistance.

In the calculation of the churning torque, many scholars have proposed different calculation models from different perspectives, but most of the existing calculation models are semi-empirical formulas obtained through experimental fitting. Comparing the calculation results of several models as shown in Fig. 5 and Table 1, and the difference between different churning torque calculation models under the same conditions is more obvious, indicating that there is still a lack

of a more unified and effective churning torque theoretical calculation model. Guo et al. [27,28] established a theoretical calculation model of gear churning resistance torque from the mechanism of gear dragging torque, using the theory of fluid attachment layer and fluid momentum theorem, taking into account the multi-parameter influence characteristics of gear transmission system, the dynamic change characteristics of gear end velocity, the dynamic change law of fluid attachment layer and the change rate of lubricant volume in the meshing area, and verified the feasibility of the model through tests.

Table 1. Comparison of churning torque calculation models

Scholars	Parameters	Deficiency
Changenet [17]	Rotational speed, lubricant density, viscosity, gear oil immersion area, lubricant volume ratio, tooth width.	The effect of helix angle was not considered in the test.
Terekhov [29]	Rotational speed, lubricant density, tooth width, gear rotation.	Low speed range.
Lauster [16]	Rotational speed, tooth width, radius, Oil immersion depth, lubricant volume ratio.	Suitable for single spur gears.

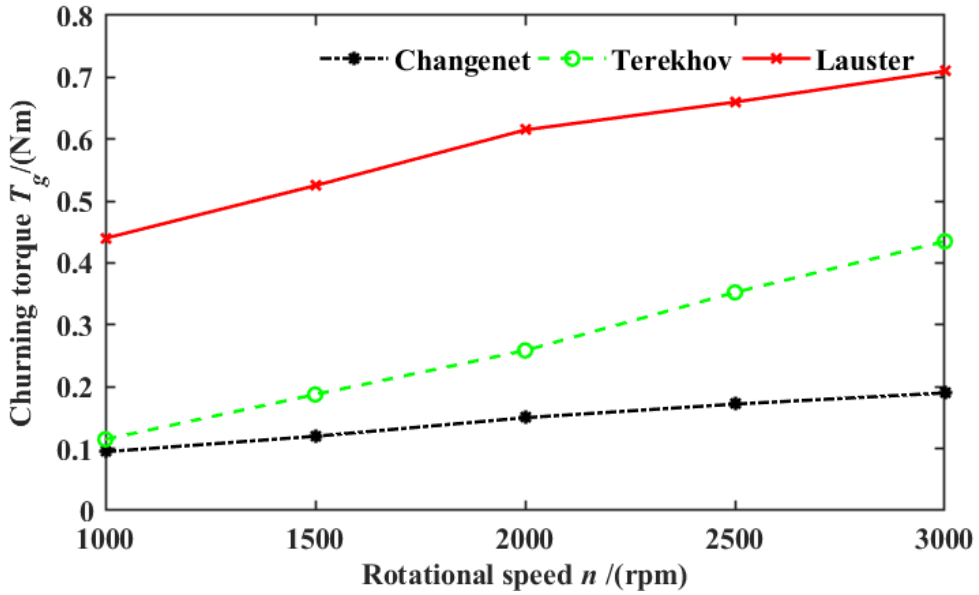

Fig. 5. Comparison of churning torque models.

The churning torque T_g is divided into three parts according to the part of the gear that acts with the lubricant in the oil-immersed state: the friction resistance torque T_{el} generated by the friction between the end face of the gear and the lubricating oil, the friction resistance torque T_w generated by the friction between the gear peripheral face and the lubricating oil, and the resistance torque T_s generated by the extrusion power loss P_s of the lubricating oil in the meshing area. In the formula, T_{el} and T_w are calculated as follows:

$$T_{el} = 2\int_0^{\sqrt{r^2-h^2}} 0.036 v^{1/5} \rho {\omega_g}^{9/5} (h^2 + l^2)^{9/5} \left(\frac{\pi\theta}{90}\right)^{4/5} dl \tag{15}$$

$$T_w = 0.036(\omega_g r)^{9/5} v^{1/5} \rho R^{4/5} B \tag{16}$$

where υ and ρ represent the kinematic viscosity and density of lubricating oil, respectively; h represents the distance between the lubricating oil surface and the gear center line; r represents the radius of gear pitch circle, w_g represents the angular velocity of gear, B represents tooth width, R represents the circumference of oil immersion. The gear churning model is shown in Fig. 6.

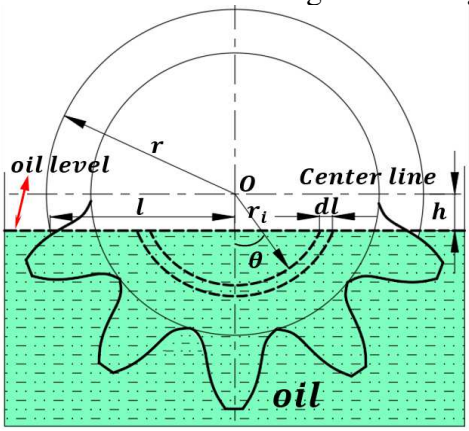

Fig. 6. Oil churning model of gear end face.

In the process of gear meshing, the teeth of the active and passive gears will periodically invade the gap area at the root of each other's teeth, causing the lubricant to be squeezed in the gear gap, resulting in a rapid decrease in the volume of the gap area and forcing the lubricant between the gear teeth to be squeezed out from the sides and the gap, thereby generating a resistive torque. Through the Boolean method of calculation to obtain each squeeze side area, and then find the backlash in the lubricant volume change and lubricant speed, the use of Bernoulli's principle to calculate the squeeze lubricant power loss, and then calculate the squeeze resistance torque. The calculation process is as follows:

$$V_{ij}^{p} = BS_{ij}^{p} \tag{17}$$

$$v_{ij}^{p} = \Delta V / S\Delta t = \left(V_{ij}^{p} - V_{ij}^{p-1}\right)\omega_i / 2S_{ij}^{p}\Delta\theta \tag{18}$$

where v_{ij}^{p} is the lubricant speed, ΔV is the volume change, Δt is the change time, B is the gear width, ω_i is the angular speed of the driven gear, and $\Delta\theta$ is the angular change, S_{ij}^{p} representing the area of the jth squeeze side of gear i at meshing position P (as shown in Fig. 7).

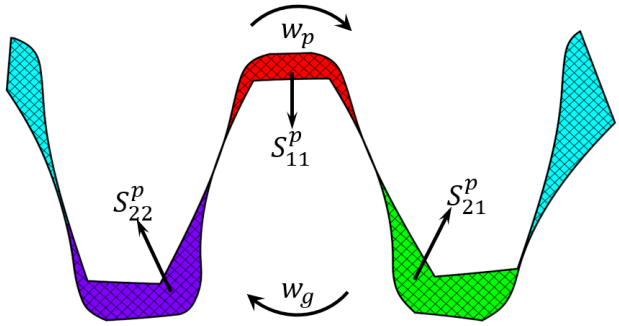

Fig. 7. Schematic diagram of extrusion area of gear pair.

The lube oil extrusion power loss is calculated as follows:

$$p_{ij}^{p} = p_{ij}^{p-1} + \frac{1}{2}\rho[\left(v_{ij}^{p}\right)^{2} - \left(v_{ij}^{p-1}\right)^{2}] \tag{19}$$

$$P_{ij}^{p} = p_{ij}^{p}\Delta V/\Delta t = p_{ij}^{p}\left(S_{ij}^{p} - S_{ij}^{p-1}\right)B\omega/\Delta\theta \tag{20}$$

The squeeze resistance torque at S_{ij}^{p} is calculated by combining in Eq. (19)-(20) as in Eq. (21)

$$T_{ij}^{p} = 9550P_{ij}^{p}/n_i \tag{21}$$

where T_i^p is the squeeze resistance torque generated by the jth squeeze side area of gear i at engagement position P, and n_i is the speed of gear i.

Similarly, calculate the lubricant squeeze resistance torque of other meshing positions, and finally find the average anti-squeeze resistance torque to obtain the average squeeze oil resistance torque of the gear, as shown in Eq. (22), where N indicates the number of squeeze side areas.

$$T_s = \frac{1}{N}\sum_{i=1}^{N} T_i^p \tag{22}$$

Therefore, the churning torque can be expressed as:

$$T_g = T_{el} + T_w + T_s \tag{23}$$

In the method of reference [30] the bearing resistive torque is shown in Eq. (24)

$$T_{rb} = \begin{cases} 10^3 f_0 (v \cdot \Delta N)^{\frac{2}{3}} {d_m}^3 & v \cdot \Delta N \geq 0.002 \\ 16\ {d_m}^3 f_0 & v \cdot \Delta N < 0.002 \end{cases} \tag{24}$$

where f_0 is the lubrication factor, which is related to the type of lubricant and lubrication method, and its value can be referred to the standard ISO TR 14179-2-2001, ΔN is the speed difference between the driven gear and the shaft; $d_m$is the average diameter of the bearing.

The oil film shear torque is mainly the resistance torque caused by the relative motion between the inner cone surface of the synchronizer lock ring and the outer cone surface of the gear friction when the synchronizer is not combined, and the mathematical expression is:

$$T_s = 4\pi^2\mu L R^3 \Delta N/30 j_c \tag{25}$$

where μ is the lubricant dynamic viscosity, L is the length of the tapered surface, R is the average radius of the tapered surface, j_c represents the clearance between the tapered surfaces of the synchronizer ring and the synchronizer gear ring.

In summary, the total no-load gear dragging torque can be expressed as:

$$T_D = T_g + T_{rb} + T_{sy} \tag{26}$$

2.4. Friction and friction torque

Due to the influence of lubricating oil and backlash, there are two kinds of friction in the process of gear meshing, namely direct contact Coulomb friction F_{ef} and hydrodynamic sliding friction F_{hf} obtained through semi-sommerfeld [31] conditions, both of which affect the dynamic characteristics of gear. According to Coulomb's law of friction, the direct contact with friction F_{ef} and its resulting torque T_{ef} can be expressed as:

$$F_{ef} = \mu(t)F_{mesh} \tag{27}$$

$$T_{ef} = F_{ef} * r_{(i)} * \sin(\alpha_t) \tag{28}$$

where $i = p, g$, and $r_{(i)}$ represents the radius of gear pitch circle, α_t represents the pressure angle of end face, $\mu(t)$ is the friction coefficient between teeth in direct contact, and the friction coefficient model proposed in Ref. [32] is shown in Eq. (29).

$$\mu(t) = 2\mu_{avg} \cdot tan^{-1}(\phi \cdot \psi)/\pi + 2\mu_{avg}\varepsilon \cdot \psi/\{\pi \cdot (1 + \phi^2 \cdot (\psi)^2)\} \tag{29}$$

where $\psi = [mod(n_p, r_{bg}, t, p_b) - L]$, and μ_{avg} is the time mean value, ϕ is the regularization factor, and $\phi = 50$ is set in this paper, p_b is the pitch of base circle, ε is gear tooth meshing coincide degree, L is the length of meshing contact line.

The hydrodynamic sliding friction F_{hf} obtained by the semi-sommerfeld condition, which is defined as follows: (where u_t is the sliding speed of tooth surface: $u_t = v_p - v_g$)

$$F_{hf} = L\pi\eta_0|u_t|\sqrt{r_{eq}}/\sqrt{2h} \tag{30}$$

Therefore, the frictional torque acting on the main and driven gears is:

$$T_{hf} = F_{hf} * r_{(i)} * \sin(\alpha_t) \tag{31}$$

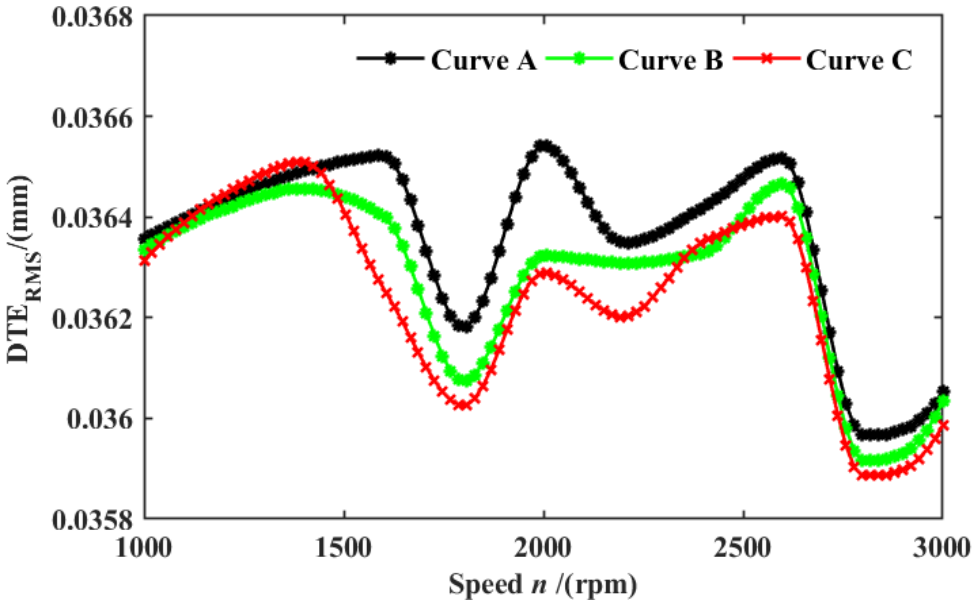

Fig. 8. RMS value of dynamic response of each model: Curve A: no friction; Curve B: Friction coefficient is constant; Curve C: time-varying friction coefficient.

In order to determine the effect of the friction coefficient on the dynamic behavior of the gear, this paper simulates three different analytical models based on frictionless contact, constant friction coefficient, and time-varying friction coefficient. The comparison results of dynamic transmission error (DTE) are shown in Fig.8. The results show that there are some frequency dependent discrepancies between these three models, but the influence is limited in general. The time-varying friction coefficient will still be used for the further analysis in this paper.

3. MODEL VALIDATION

In order to verify the accuracy of the proposed model, the dual-clutch transmission was tested on the three-motor test stand (Fig. 9) to obtain test data. Considering that the coupling between the power flow gear and the no-load or light-load gear is not strong, the whole dual-clutch transmission is selected for the test. The main motor of the stand is directly connected to the transmission using a rigid shaft, so that the 2nd order engine excitation simulated by the N/T control mode control motor to be transferred directly to the transmission input shaft, outputting a continuously fluctuating speed, and the two secondary motors are connected to the two half shafts of the transmission to simulate the load torque. Most transmission bench tests collect vibration and noise signals, which makes it difficult to compare with the simulation results. In this study, a magnetoelectric speed sensor is used to measure the gear speed and angular acceleration can be obtained.

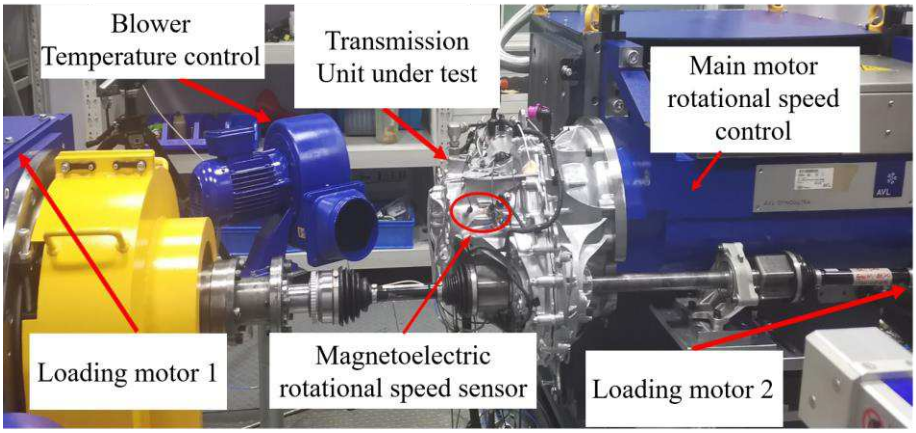

Fig. 9. Transmission test bench and speed sensor installation position.

The motor parameters and test conditions are shown in Table 2, and the model dynamic response is calculated under the condition that the test conditions and simulation conditions are consistent, and the angular acceleration amplitude α_g of a gear at the 2nd order excitation frequency is compared with the test analysis results. It should be noted that the test and simulation results are filtered to ensure that 50 Hz is the main characteristic frequency, and the comparison results are shown in Fig. 10.

Table 2. Motor parameters and test conditions.

	Motor	Max/Rated speed	Max Torque	Power
Motor parameters	Main motor	10000/5435rpm	650Nm	370 kw
	Secondary motor	3000/650rpm	3200Nm	220 kw
Test conditions	Input speed	1500rpm		
	Angular acceleration	Increase from 0 to 1500 rad/s^2in 0-90s		
	Input torque	80 Nm		

From the Fig. 10, it can be found that the trend of the simulation results and the test results are in good agreement, and it is worth noting that the simulation results are slightly smaller in value than the test results, and there is a certain error in the amplitude. There are two possible reasons for the error: (1) it is related to the vibration of the table and the installation of the gearbox,

and as the fluctuation amplitude increases, it causes the vibration of the test bench and the transmission input shaft to increase, resulting in large test results; (2) the dynamics model established is somewhat simplified compared with the actual one. However, the errors on the results are within the acceptable range. Therefore, the simulation results are basically consistent with the results of the bench test, which verifies the validity of the built single-tooth rattle dynamics model, which can be used for further parametric analysis.

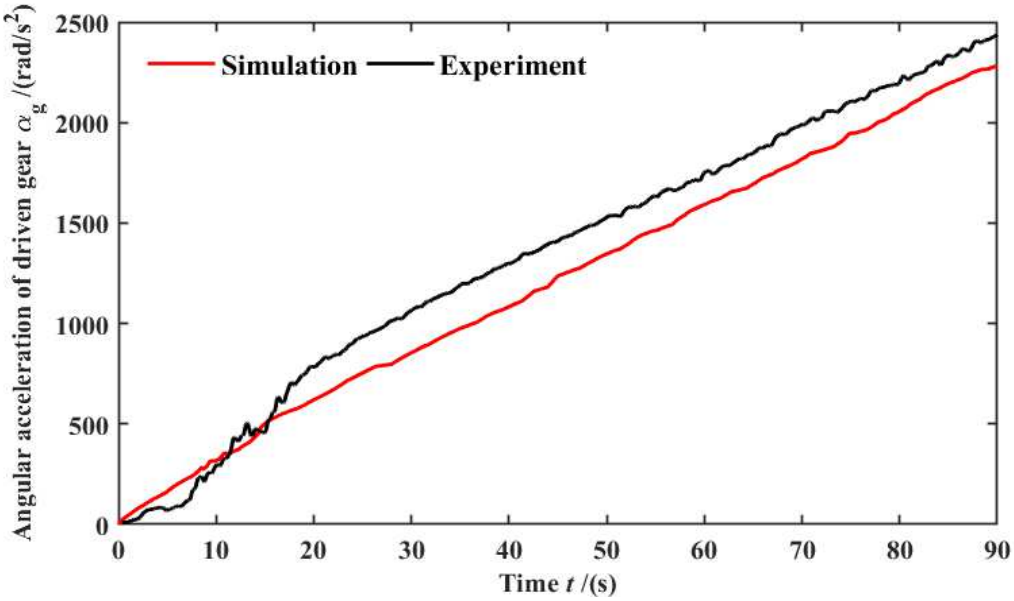

Fig. 1. Comparison of angular acceleration of loose gears

4. NUMERICAL SIMULATIONS AND ANALYSIS.

The main factors affecting gear rattle include input excitation and torque fluctuation, drag torque, and lubricant viscosity, etc. It is important to find out the nonlinear response and parameters of the system under the effect of each parameter to suppress the occurrence of gear rattle. In this section, the validated single tooth rattling dynamics model is used to solve the equations using the 4th order Runge-Kutta method with variable step size to obtain the bifurcation diagram and relative displacement time domain, frequency domain, phase trajectory and Poincare mapping of the system under different influencing factors, and the Jerk (derivative of force with respect to time) based rattling indicator as shown in Eq. (32) is selected to evaluate the parameter variation with reference to literature [33]. The effect on the rattle strength of the gear is analyzed by the forward difference method for the sensitivity of the rattle index, as shown in Eq. (33).

$$RI = \dot{F}_{mesh\,,RMS}/I_g \tag{32}$$

$$\frac{\partial RI}{\partial X_{\mathrm{i}}} = \frac{RI(X_{\mathrm{i}}) - RI(X)}{\Delta X_{\mathrm{i}}} \tag{33}$$

where $\dot{F}_{mesh}$ is the derivative of gear meshing force to time, $\partial RI/\partial X_{\mathrm{i}}$ represents the rattle sensitivity, the larger the value of RI, the more obvious the change of tooth meshing force, the more intense the tooth impact, and the more serious the rattling phenomenon.

4.1. Excitation frequency

Under different excitation frequencies, the dynamic response of the system exhibits rich vibration characteristics, which have a non-negligible impact on the rattle phenomenon of transmission gears. Therefore, in order to analyze the effect of input excitation frequency on the rattle nonlinear characteristics of the gear vice, the response results at f_m of 10, 25, 50 and 60 Hz are compared without loss of generality, and the rattling strength at different input excitation frequencies is visually compared by the rattle index *RI*, and the simulation analysis results have typical nonlinear dynamic characteristics. In order to highlight the comparability, the numerical calculation is set with a gear backlash of 0.12 mm, a drag torque of 0.1 Nm, an input angular acceleration of 300 rad/s^2, a dynamic viscosity of 0.01$p_a \cdot s$.

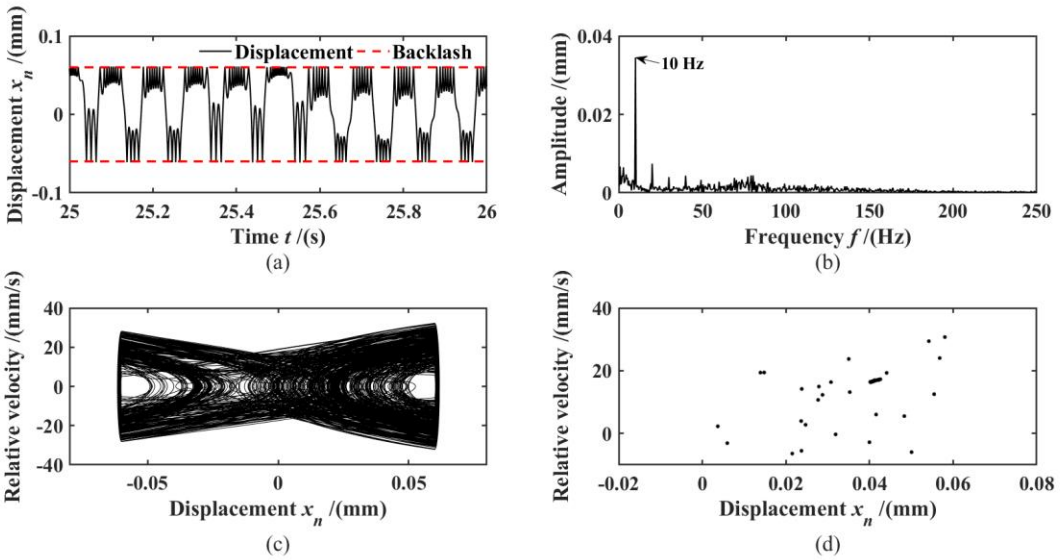

Fig. 11. Dynamic response (f_m=10Hz): (a) relative displacement; (b) Fourier spectrum; (c) phase diagram; (d) Poincare map.

As shown in Figs. 11-12, when f_m is 10 Hz and 25 Hz, the wheel teeth are impacted on both the driven and non-driven sides, the relative displacement x_n oscillates between the gear backlash, and the gears produce double-sided rattle, but the contact between the wheel teeth and the non-driven side is relatively less when f_m is 25 Hz. The Fourier spectrum diagram shows that the input excitation frequency component has the largest contribution to x_n, and the spectrum at 25Hz is a continuous spectrum with a certain width; the system appears chaotic response in both cases, the time course of the response is a non-periodic response, the phase trajectory is a closed curve with a certain width, the Poincare cross section is distributed in multiple discrete points, and the motion is chaotic motion, which can be It can be seen that the system vibration response increases sharply after the chaos increases.

When f_m is 50 Hz, as shown in Fig. 13, the system is a periodic response, and the time courses of the responses are all periodic. It can be seen by the spectrogram that the Fourier spectrum is distributed over discrete points of $kf_m/2$ (k is a positive integer and f_m is the excitation frequency), and the periodic solution of the system is quite rich in super-harmonic and subharmonic components, and the phase trajectory is a non-elliptical closed curve. Poincare cross section presents 2 points distributions respectively, and the system motion is periodic. And when

f_m is 60 Hz, as shown in Fig. 14, the system appears chaotic response, the time course is non-periodic motion, the Poincare cross-section presents multiple discrete point distributions.

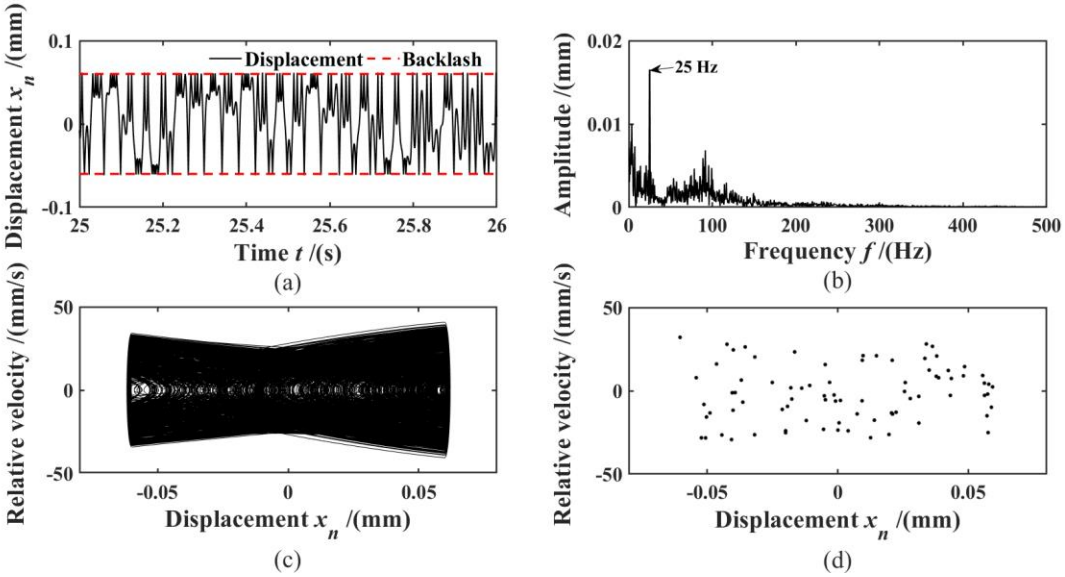

Fig. 12. Dynamic response (f_m=25Hz): (a) relative displacement; (b) Fourier spectrum; (c) phase diagram; (d) Poincare map.

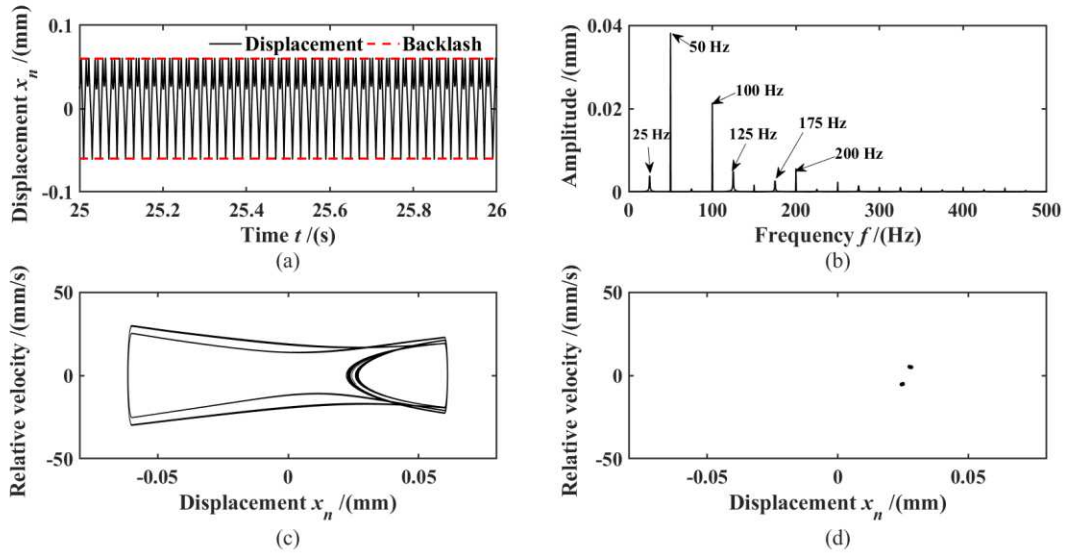

Fig. 13. Dynamic response (f_m=50Hz): (a) relative displacement; (b) Fourier spectrum; (c) phase diagram; (d) Poincare map.

Comparing the system response results generated by different excitation frequencies, it shows that the impact frequency of tooth face changes with the increase of excitation frequency; in each cycle under low excitation frequency, multiple impacts occur on the driving face as well as on the non-driving face, and in each cycle under higher excitation frequency, only one impact occurs on the driving face as well as on the non-driving face. It indicates that the excitation frequency is an important factor that causes the tooth surfaces to detach from each other and produce rattle; looking at the whole process of the system response, its motion state experiences

chaotic to periodic and chaotic motion, and the nonlinear performance of the rattle dynamics of the gear pair coupled with multiple nonlinear strong factors is obvious.

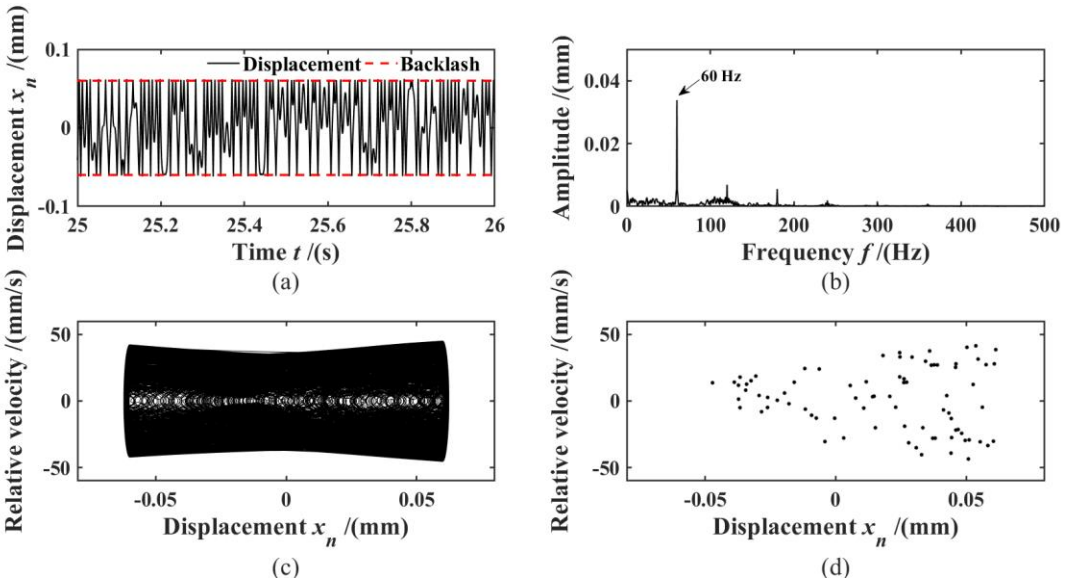

Fig. 14. Dynamic response (f_m=60Hz): (a) relative displacement; (b) Fourier spectrum; (c) phase diagram; (d) Poincare map.

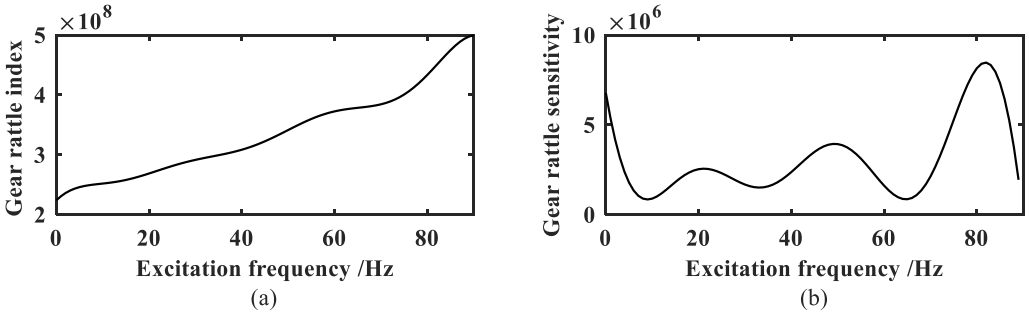

Fig. 15. (a) Rattle evaluation index *RI*; (b) Rattle sensitivity.

The rattle index *RI* and rattle sensitivity of the system when the input excitation frequency increases from 0 to 90 Hz are also calculated as shown in Fig. 15. The rattle index shows a monotonically increasing trend, indicating that the higher the input excitation frequency, the higher the high-frequency impact strength increases and the gear rattle intensifies, and the rattle sensitivity is greater than 0, indicating that the *RI* is positively correlated with the excitation frequency. Therefore, choosing a suitable input excitation frequency can prevent the system from entering a chaotic state, which helps to reduce the gear rattle strength, and improve the stability and NVH performance of the system.

4.2. Fluctuation amplitude of Input torque

When there are periodic fluctuations of input torque, it may lead to different degrees of rattle of the gear pair. Therefore, in order to analyze the effect of the amplitude of input torque fluctuation on the rattle nonlinear characteristics of the gear pair, the response results at α_0 of 0,

100, 250 and 320 rad/s^2 are compared without loss of generality, and the rattle index RI is used to visually compare the rattle strength at different amplitudes of input torque fluctuation The results of the simulation analysis have typical nonlinear dynamic characteristics. To highlight the comparability, the backlash of 0.12mm, drag torque of 0.1Nm and dynamic viscosity of $0.01p_a \cdot s$ are set for the numerical calculation.

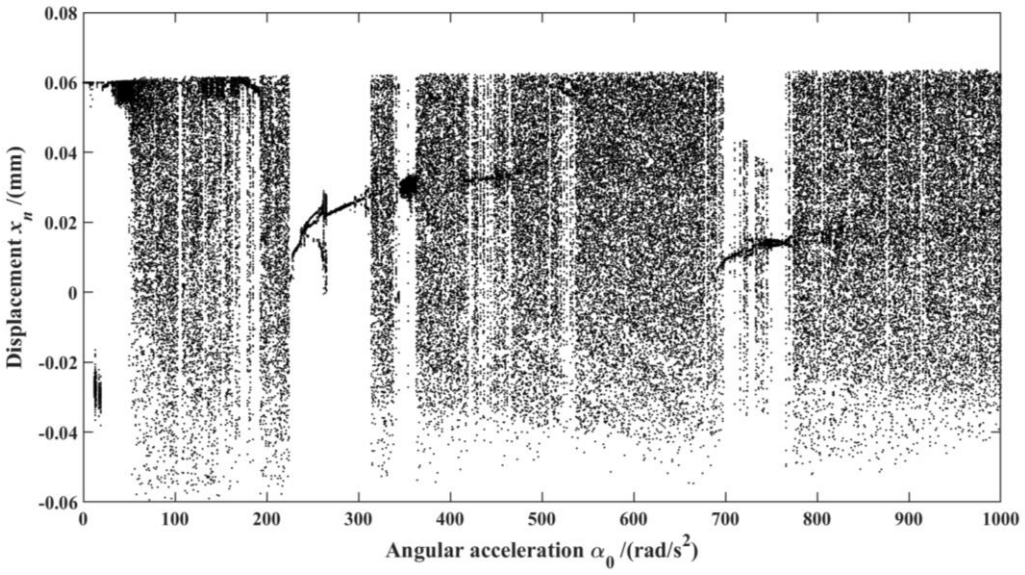

Fig. 16. Bifurcation of the system with the amplitude of input torque fluctuations.

As shown in Fig. 16, during the change of input angular acceleration amplitude, the whole system motion is chaotic motion. In the region of chaotic motion, there exists periodic motion, i.e., chaotic motion alternates with periodic motion, and there exists a window of periodic motion in chaotic motion. For example, the system exhibits periodic motion in a small region of angular acceleration amplitude of 218-300 rad/s^2, and these periodic motions are a window of periodic motion in chaotic motion. In terms of the number of periodic solutions, as the angular acceleration increases, the system starts to bifurcate from a single cycle after excitation to a multiplicative cycle, with single cycle, 3-cycle motion, etc., and the system amplitude decreases significantly. After α_0 is 300 rad/s^2 the system starts to decay until the generation of chaotic motion.

In Fig. 17, when α_0 is 0 rad/s^2, the system is a quasi-periodic response, the time course of the response is non-periodic response, due to the time-varying characteristics of the gear mesh stiffness, non-linear oil film force leads to the existence of oscillations in the relative displacement, but x_n is always greater than 0, the amount of oscillation is very small, indicating that the gear is in a normal meshing state in this case, the teeth are only in contact on the drive side, there is no rattle produced. The Fourier spectrum is distributed at discrete points at 425 Hz, (k is a positive integer, f_m is the excitation frequency), indicating that the system response contains a super harmonic response. When α_0 is 100 rad/s^2, as shown in Fig. 18, the time course of the system response is non-periodic response, and the gear oscillates more obviously with respect to the displacement x_n, and there is a more obvious phenomenon of tooth disengagement, but the value of x_n is still greater than 0, at this time, the impact-disengagement cycle occurs repeatedly on the driving side of the gear teeth, and there is no contact with the non-driving side, which is shown as single-sided rattle, and the system motion is chaotic.

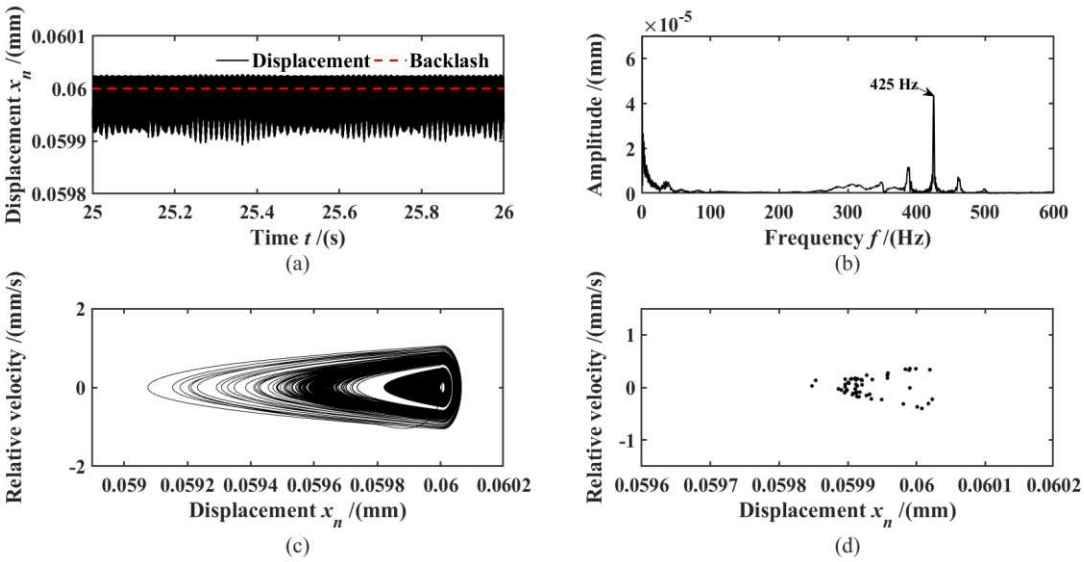

Fig. 2. Dynamic response ($\alpha_0 = 0 rad/s^2$): (a) relative displacement; (b) Fourier spectrum; (c) phase diagram; (d) Poincare map.

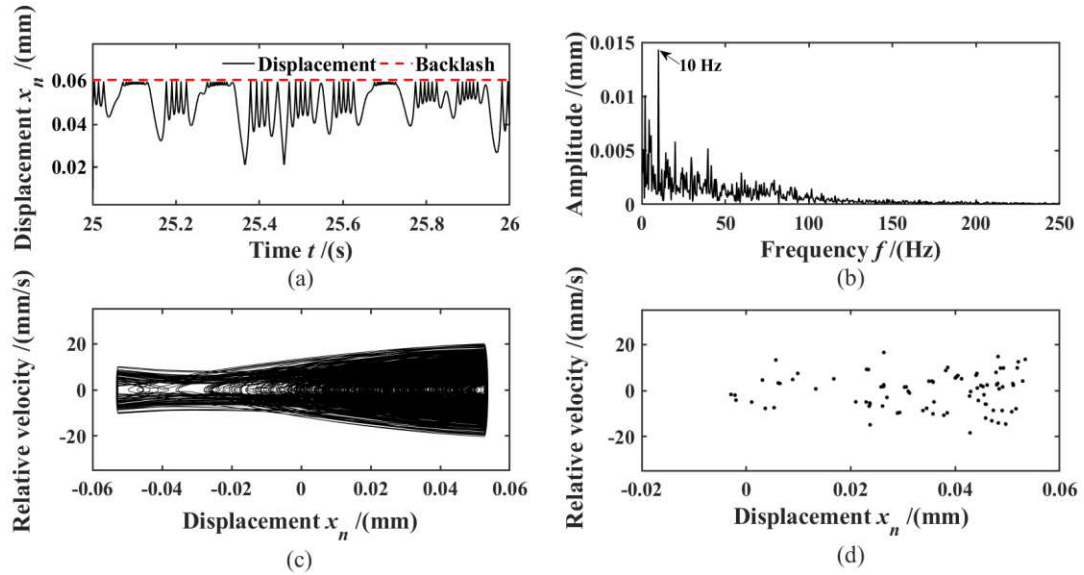

Fig. 18. Dynamic response ($\alpha_0 = 100 rad/s^2$): (a) relative displacement; (b) Fourier spectrum; (c) phase diagram; (d) Poincare map.

When α_0 is 250 rad/s^2, the system response is shown in Fig. 19, and the system is a times-periodic response, and there are high frequency shocks in the gear wheel teeth on the driving side and the non-driving side, and in one excitation cycle, the gear first produces a series of shocks on the driving side, and under the action of inter-tooth lubricant, the shocks gradually decay to Then transition to the non-driven side, and then produce a series of shocks with gradually decreasing strength, at this time, the relative displacement x_n oscillates between the gear backlash, and the gear produces double-sided rattle. The system phase trajectory is a closed curve with a certain width, and the Poincare section is distributed in three discrete points, and the system motion is

periodic. Continuing to increase the angular acceleration amplitude, the system response is shown in Fig. 20, and the system again appears chaotic response. Throughout the whole process of the system response, its motion state goes through the process of period, bifurcation, and chaos, and comparing the dynamic response in these previous cases shows that the input fluctuation is an important factor that causes the tooth surfaces to detach from each other and produce rattle.

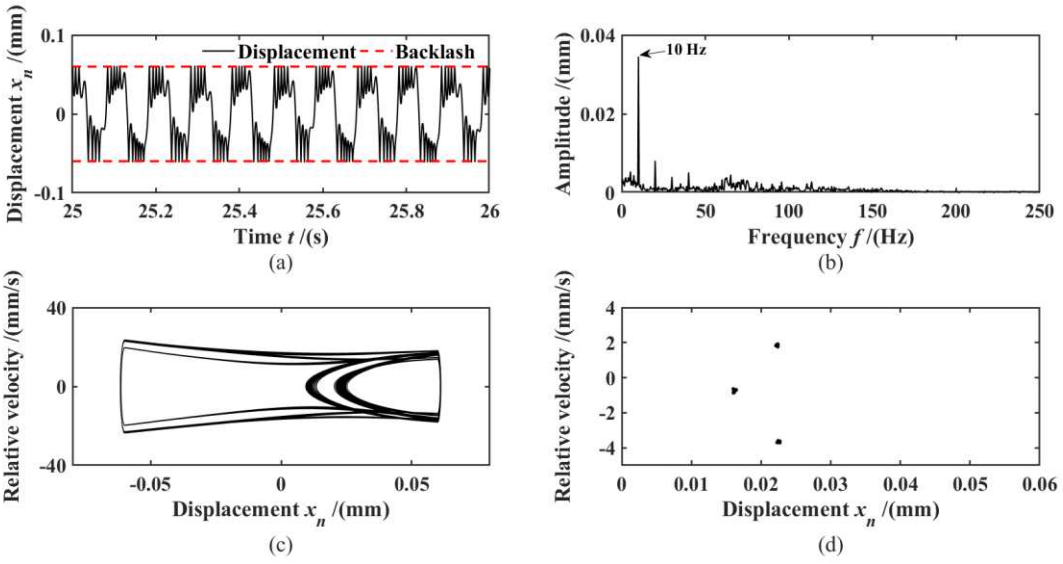

Fig. 19. Dynamic response ($\alpha_0 = 250 rad/s^2$): (a) relative displacement; (b) Fourier spectrum; (c) phase diagram; (d) Poincare map.

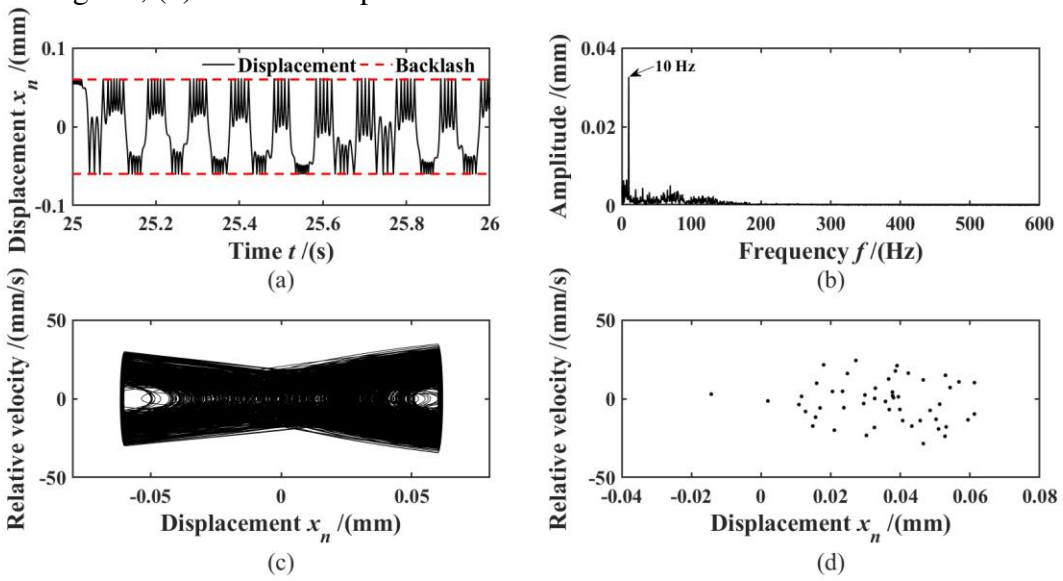

Fig. 20. Dynamic response (α_0=320rad/s^2): (a) relative displacement; (b) Fourier spectrum; (c) phase diagram; (d) Poincare map.

The rattle index *RI* and rattle sensitivity of the system when α_0 is increased from 0 to $1000 rad/s^2$ are also calculated as shown in Fig. 21. The rattle index shows a monotonically increasing trend, with the increase of α_0, the vibration amplitude of the system gradually increases and the system torque fluctuation intensifies, making rattle more likely to occur, and the gear rattle

sensitivity are greater than 0, indicating that RI is positively correlated with α_0. Therefore, appropriately reducing the input torque fluctuation amplitude can prevent the system from entering the chaotic state, and help reduce or suppress the gear rattle strength to improve the stability and NVH performance of the system.

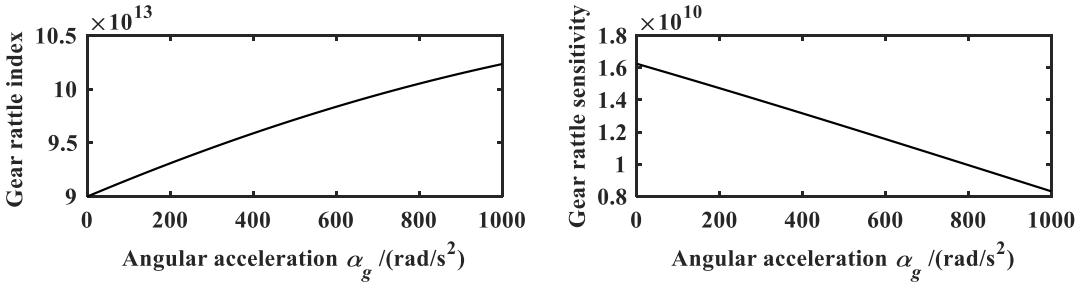

Fig. 21. (a) Rattle evaluation index RI; (b) Rattle sensitivity.

4.3. Drag torque

The drag torque T_D has the effect of impeding the rotation of the hollow-sleeve gear and can weaken the tendency of tooth surface separation, which is one of the important factors affecting the occurrence of rattle, and the effect of different drag torque on transmission gear rattle will not be negligible. Therefore, without loss of generality, the bifurcation of the system with the variation of the drag torque is calculated, and the response results are compared for T_D of 0.1, 0.3 and 0.44Nm, and the rattle strength under different input torque fluctuation amplitudes is visually compared by the rattle indicator RI. To highlight the comparability, the numerical calculation was set with a backlash of 0.12mm, an angular frequency of torque fluctuation of 50Hz (i.e. w=100π rad/s), an input angular acceleration of 300 rad/s, and a kinetic viscosity of 0.01$p_a \cdot s$.

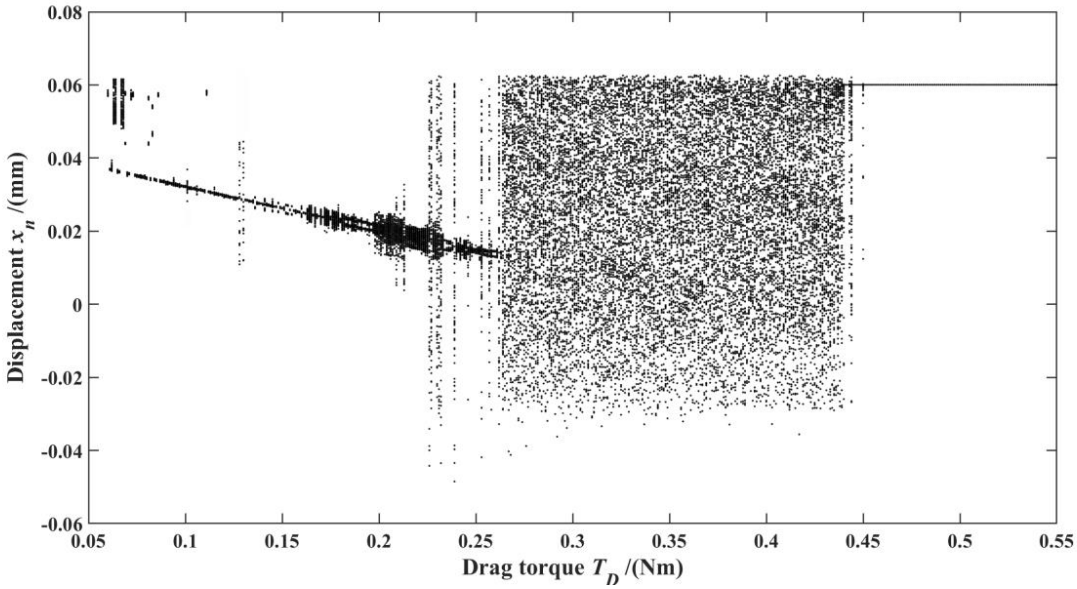

Fig. 22. Bifurcation of the system with the variation of the dragging torque.

The Fig. 22 shows that in the process of towing torque change, the system motion changes from periodic motion to chaotic motion, and the system exhibits periodic motion in the small

region of the dragging torque of 0.08-0.16 Nm, these periodic motions are a window of periods in chaotic motion. After T_D is 0.16Nm the system starts to decay until the generation of chaotic motion. When T_D is greater than 0.44Nm, the relative displacement is always greater than the gap value, and the teeth are only in contact on the drive side, and the system tends to stabilize. The overall system with the change of the dragging torque, its periodic motion is not obvious, will be faster transition to the quasi-periodic and chaotic state, in the large dragging torque, the tendency of the empty set gear tooth surface to occur separation is further weakened, and finally the system into a stable single-cycle state.

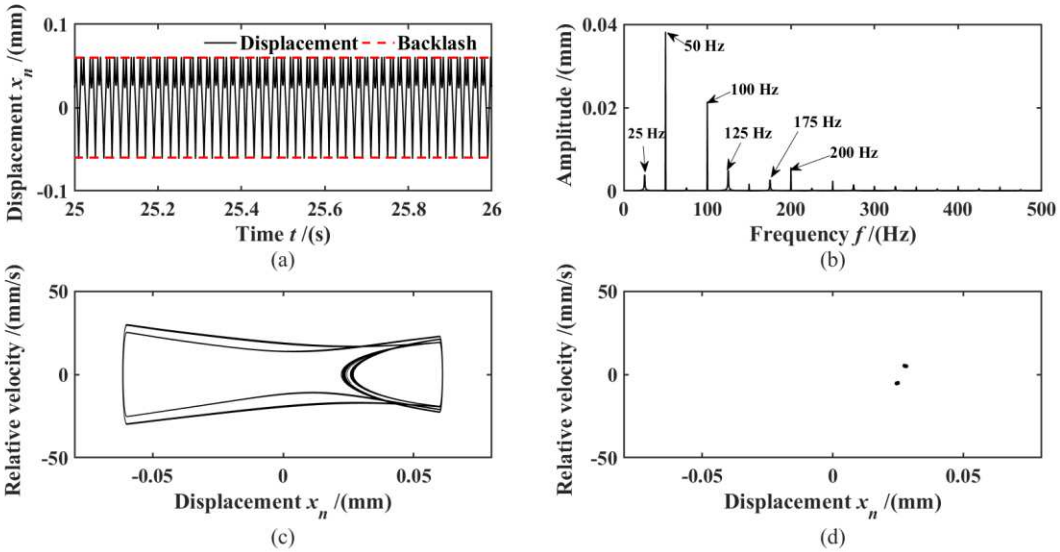

Fig. 23. Dynamic response (T_D=0.1Nm): (a) relative displacement; (b) Fourier spectrum; (c) phase diagram; (d) Poincare map.

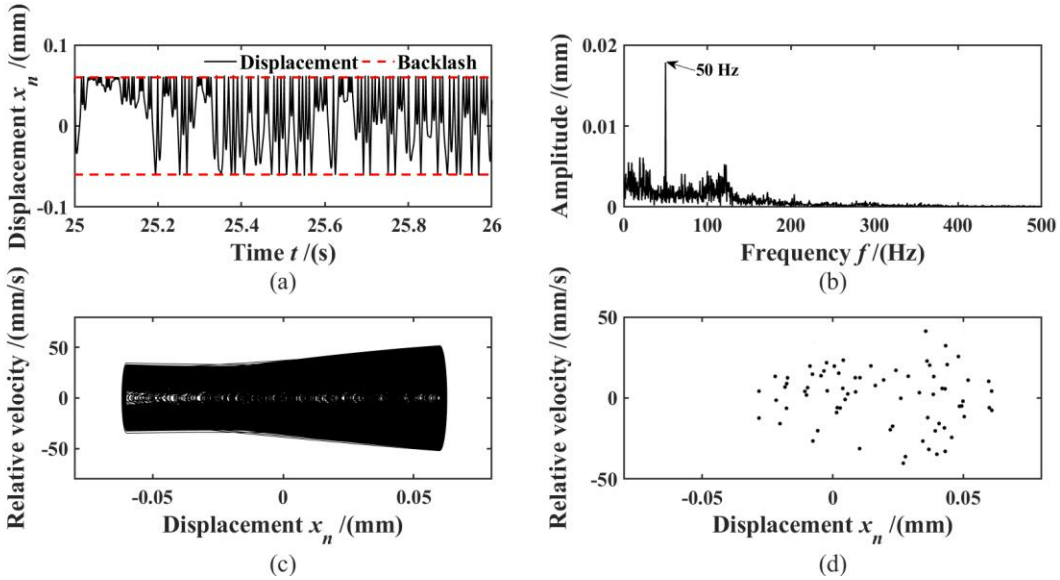

Fig. 24. Dynamic response (T_D=0.3Nm): (a) relative displacement; (b) Fourier spectrum; (c) phase diagram; (d) Poincare map.

As shown in Fig. 23, when T_D is 0.1Nm, the response of the system is a non-simple harmonic periodic second harmonic response, the relative displacement x_n oscillates between the backlash, and the wheel teeth are impacted on both the driven and non-driven sides, which behaves as two-sided rattle. The Fourier spectrum is distributed on the discrete points of $kf_m/2$, and the frequency component of 50Hz has the largest contribution to x_n. Poincare cross section is distributed in two points, and the system motion is periodic.

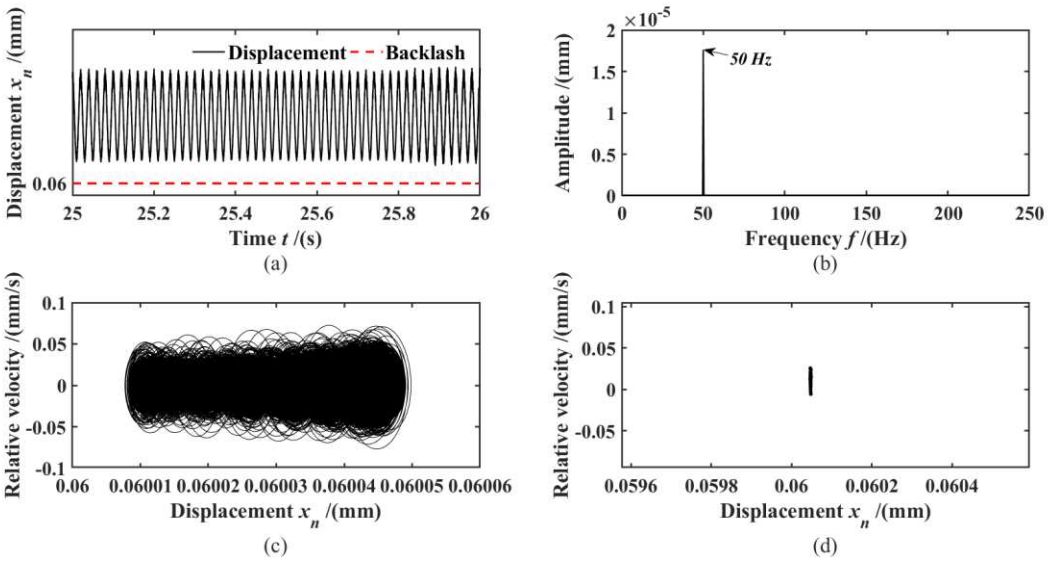

Fig. 25. Dynamic response (T_D=0.44Nm): (a) relative displacement; (b) Fourier spectrum; (c) phase diagram; (d) Poincare map.

When T_D is 0.3Nm, the system response is shown in Fig. 24, and the chaotic response starts to appear, the time course of the response is non-periodic motion, the gear teeth are impacted on both the driving and non-driving sides, and there is the phenomenon of dislocation, and the meshing process is mixed with one-sided rattle (driving side), because the increase of the dragging torque makes the gear teeth not easy to separate, and the gear teeth are rattled more on the driving side, which reduces the degree of double-sided rattle of the gear vice, but the overall performance is double-sided rattle. When T_D is 0.44Nm, as shown in Fig. 25, the system responds to the quasi-periodic motion, the relative displacement of gears is greater than the clearance value, the gears are in the normal meshing state, and no rattle occurs on the gears. It is found that with the increase of the dragging torque, the gears gradually transition from double-sided rattle to single-sided rattle, and finally stabilize and no more rattle occurs.

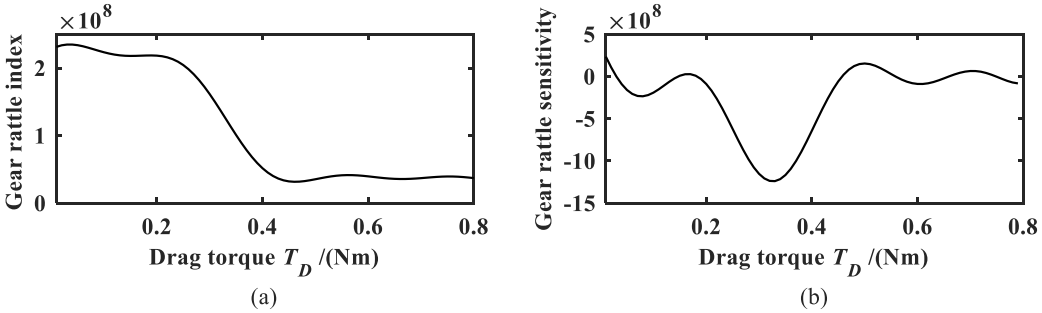

Fig. 26. (a) Rattle evaluation index RI; (b) Rattle sensitivity.

The rattle index *RI* and rattle sensitivity of the system when T_D increases from 0 to 0.8 Nm are also calculated as shown in Fig. 26. The rattle index shows a monotonically decreasing trend, with the increase of T_D, the vibration amplitude of the system gradually increases, and the teeth are gradually difficult to separate, which makes rattle less likely to occur, and the rattle sensitivity are less than 0, which means that *RI* is negatively correlated with T_D. Therefore, the appropriate dragging torque is helpful to prevent the system from entering the chaotic state, and at the same time, it can effectively reduce or inhibit the occurrence of gear rattle to improve the stability and life of the system.

4.4. Dynamic viscosity

When the tooth surfaces are not in contact, the lubricant in the gear backlash can be equated to an elastic-damping element, and the change of lubricant viscosity can be regarded as the change of the stiffness of the elastic-damping element as well as the damping coefficient, which has a non-negligible effect on the rattle phenomenon of the gear. Therefore, in order to investigate the effect of lubricant viscosity on the nonlinear characteristics of gear rattle, without loss of generality, the system is calculated with the change of the lubricant dynamic viscosity. The response results are compared for η_0 of 0.01, 0.024 and $0.03\,p_a \cdot s$, and the rattle strength at different lubricant viscosities is visually compared by rattle index *RI*, and the simulation analysis results have typical nonlinear dynamic characteristics. It should be noted that the dynamic viscosity also affects the magnitude of the dragging torque, and in order to compare the effect of different dynamic viscosities on the system, therefore, the effect of viscosity on the dragging torque is not considered in this section.

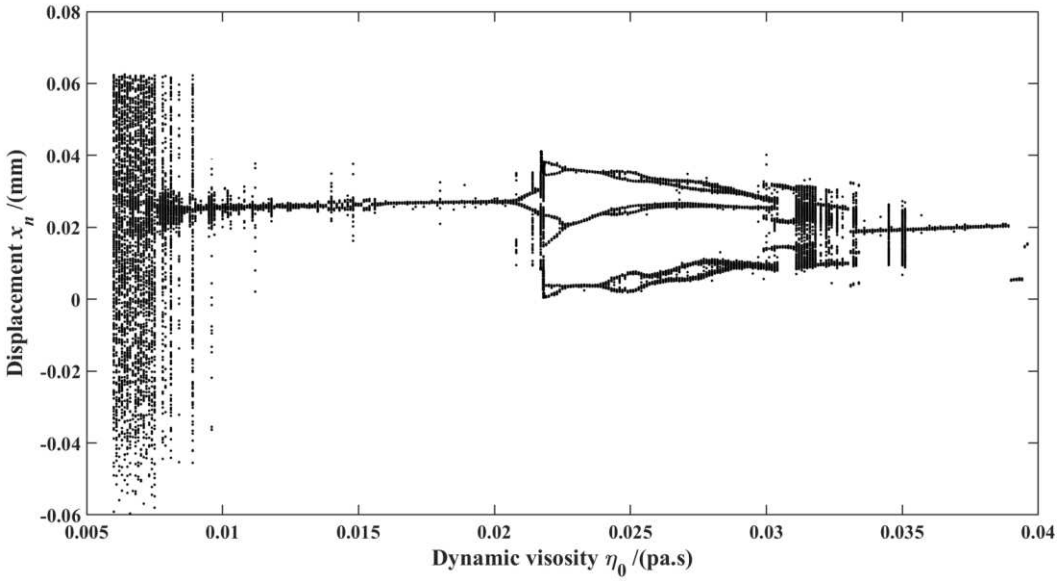

Fig. 27. Bifurcation of system with dynamic viscosity of lubricating oil.

As shown in Fig. 27, during the change in the dynamic viscosity of the lubricant, the system motion evolves from the initial chaotic state to periodic motion and then to chaotic motion, and in the region of chaotic motion, there exists periodic motion, that is, chaotic motion alternates with periodic motion, and there exists a window of periodic motion in chaotic motion. The system

exhibits periodic motion in the region to the left of η_0 of 0.0219 and in the small segment of 0.031-0.0318. These periodic motions are a periodic window in the chaotic motion, and there are many such periodic windows throughout the process of dynamic viscosity change. From the number of periodic solutions, as the kinetic viscosity increases, the system starts to bifurcate from a single cycle to a multiple cycle after the excitation, and there are 3-cycle and 6-cycle motions, which further show the rich and diverse bifurcation characteristics of the system, and when η_0 is 0.0318, the system reenters the chaotic state, and after η_0 is 0.0336, the system starts to reverse the bifurcation to a stable single-cycle state.

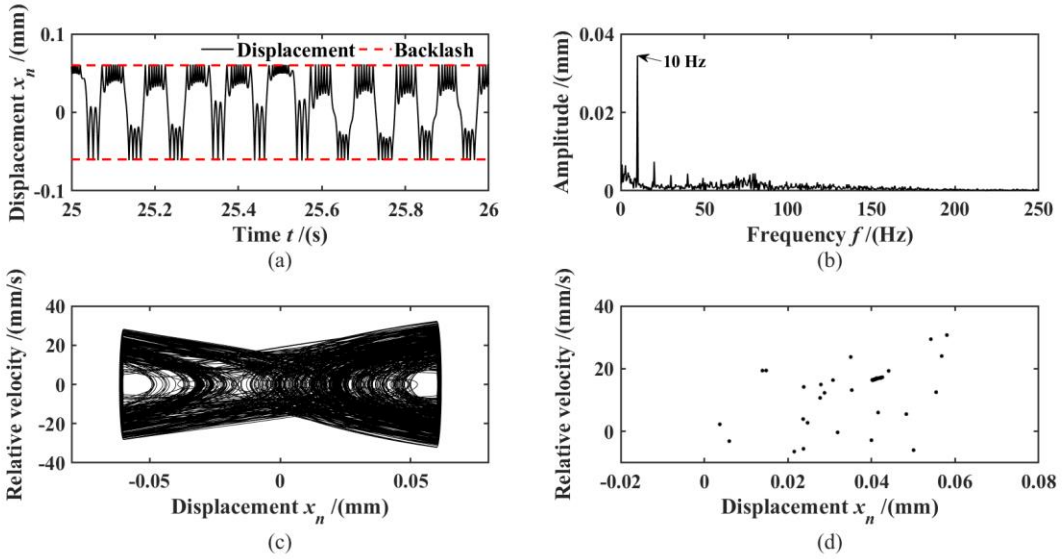

Fig. 28. Dynamic response (η_0=0.01$p_a \cdot s$):(a) relative displacement; (b) Fourier spectrum; (c) phase diagram; (d) Poincare map.

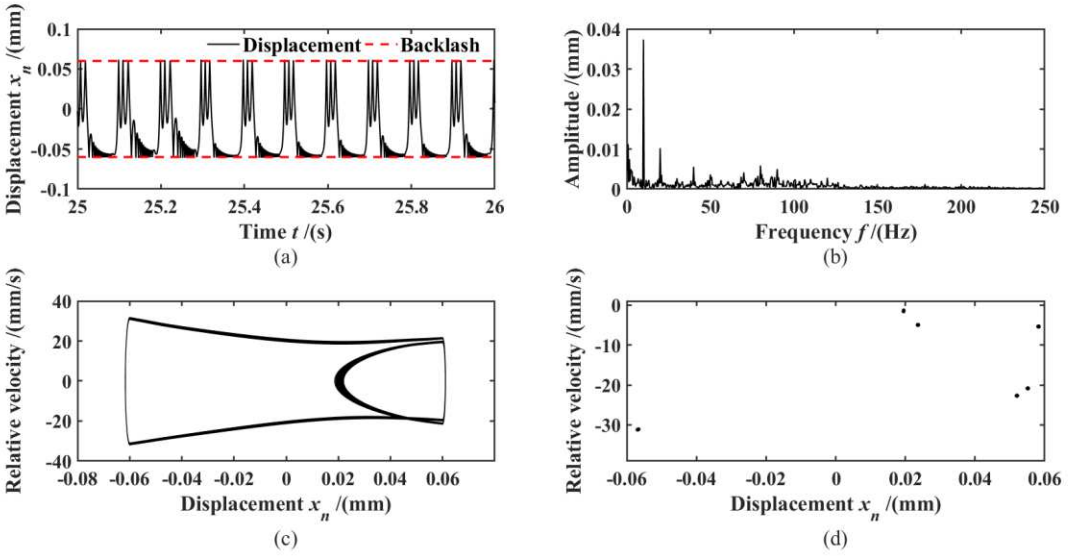

Fig. 29. Dynamic response (η_0=0.024$p_a \cdot s$):(a) relative displacement; (b) Fourier spectrum; (c) phase diagram; (d) Poincare map.

As shown in Figs. 28-29, when the lubricant viscosity η_0 is $0.01p_a \cdot s$, the system has a chaotic response, the time course of the response is non-periodic motion, the wheel teeth are impacted on both the driving and non-driving sides, the relative displacement x_n oscillates between the backlash, the system mainly occurs double-sided rattle, the Poincare cross-section is distributed by several discrete points, when η_0 is $0.024p_a \cdot s$, the system response is times periodic motion, the phase trajectory is a closed curve with a certain width, and the Poincare section is distributed by six discrete points. In Fig. 30, when η_0 is $0.03p_a \cdot s$, the system is chaotic response, the time course of the response is non-periodic motion, the phase trajectory is a closed curve with a certain width, the Poincare cross-section is distributed by several discrete points, and the system motion is chaotic motion.

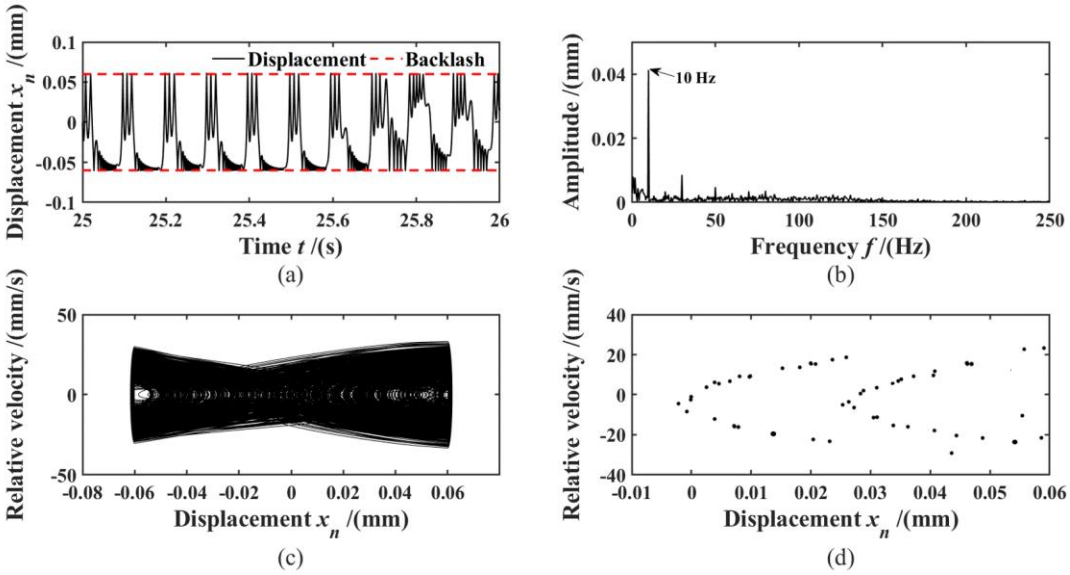

Fig. 30. Dynamic response (η_0=$0.03p_a \cdot s$):(a) relative displacement; (b) Fourier spectrum; (c) phase diagram; (d) Poincare map.

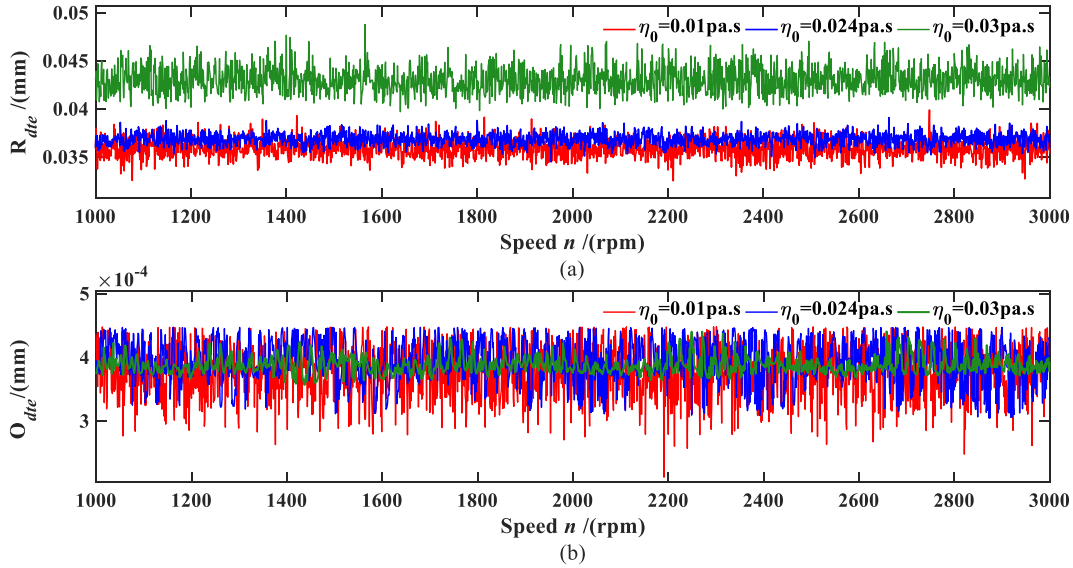

Fig. 31. (a) RMS value; (b) Oscillatory component of the transfer error.

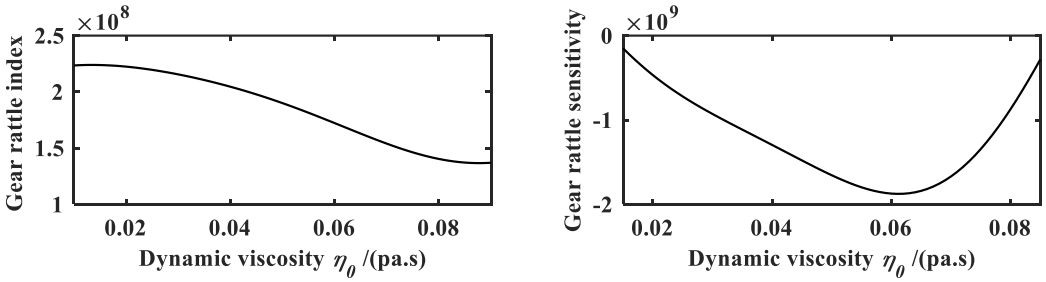

(a) (b)

Fig. 32. (a) Rattle evaluation index *RI*; (b) Rattle sensitivity

At the same time, the RMS value of the transfer error R_{dte} at a specific speed and the oscillatory component of the transfer error O_{dte} are also defined as in Eq. (34-35), where N is the total time step used for the numerical calculation, which is 5 × 10^6 in this study.

$$R_{dte} = \sqrt{\sum_{ij}^{N}(DTE_{ij})^2} \tag{34}$$

$$O_{dte} = \sqrt{\frac{1}{N}\sum_{ij}^{N}(DTE_{ij+1} - DTE_{ij})^2} \tag{35}$$

Numerical calculation of the three viscosities of R_{dte} and O_{dte} comparison results are shown in Fig. 31 , while combined with the rattle index *RI* and rattle sensitivity as shown in Fig. 32 can be found, the greater the viscosity of the lubricant, the stronger the damping effect of the squeeze film, the curve overlap range and peak with the increase in viscosity and decrease, the more rapid the decay of high frequency impact strength, and *RI* is monotonically decreasing trend, while rattle sensitivity are greater than 0, *RI* and η_0 is positively correlated. It shows that lubricant viscosity has a great influence on the dynamic characteristics of gears. Larger dynamic viscosity accelerates the decay of impact force, but excessive dynamic viscosity affects mechanical efficiency, therefore, appropriately increasing the dynamic viscosity can effectively prevent the system from entering a chaotic state, which helps to reduce or inhibit gear rattle strength, and improve the stability and NVH performance of the system.

5. SUMMARY

In this paper, a nonlinear gear rattle model is proposed, which considers time-varying friction forces and other strong nonlinear factors such as time-varying meshing stiffness, meshing damping, gear backlash and oil film force. The proposed model is verified by three-motor drive test. The nonlinear dynamic characteristics is studied by analyzing the time history of response, phase trajectory diagram, Poincare cross section and Fourier spectrum, and based on the gear rattle index, the influence of each parameter is analyzed, and the following conclusions are given:

1. The model is validated by a dual-clutch transmission bench test. The numerical calculation result of the model has good consistency with the change trend of the test result calculated angular acceleration is in good consistency with the test results, and the numerical error is within the acceptable range. The model can accurately reflect the rattle phenomenon of the gear with good accuracy.

2. As the lubricant viscosity increases, the system shows periodic, bifurcation and chaotic behavior alternately, At the same time, the larger the viscosity, the greater the equivalent damping of the system, the high frequency shock intensity decays more rapidly due to large drag torque,

which can effectively suppress or reduce the occurrence of gear rattle. Therefore, appropriately increasing the dynamic viscosity can effectively prevent the system from entering the chaotic state, reduce the gear rattle strength.

3. With the increase of the torque fluctuation amplitude α_0, the system has experienced the evolution process of quasi-periodic, bifurcation, period doubling and chaos, and the system exhibits rich and diverse bifurcation characteristics. Gear rattle index increases with the amplitude of input angular acceleration fluctuation, and reducing the input torque fluctuation of gear pair, which has a positive effect on controlling the occurrence of gear rattle, and can prevent the system from entering a chaotic state.

4. The input excitation frequency and the drag torque likewise have a great influence on the nonlinear behavior of the system, and the system undergoes both periodic and chaotic motions as the parameters change. However, with large drag torque, the tendency of tooth separation is further attenuated and the system eventually enters a stable single-cycle state. Therefore, a larger drag torque is beneficial to prevent the system from entering the chaotic state, which can effectively reduce or inhibit the occurrence of rattle.

ACKNOWLEDGEMENTS

This project was supported by National Natural Science Foundation of China (Grant No. 51975080, 52005067), Natural Science Foundation Project of Chongqing Science and Technology, Commission (Grant No. cstc2019jcyj-msxmX0733), the Science and Technology Research Program of Chongqing Municipal Education Commission (Grant No. KJQN201901121), and Youth project of science and technology research program of Chongqing Education Commission of China (No. KJQN201901115) .

Thanks to Magna PT Powertrain (Jiangxi) Co., Ltd for providing the bench test to this research project.

DATA AVAILABILITY STATEMENTS

The datasets generated during and/or analysed during the current study are available from the corresponding author on reasonable request.

COMPLIANCE WITH ETHICAL STANDARDS

Conflict of interest: The authors declare that there is no conflict of interest.

REFERENCES

[1] K. Karagiannis, F. Pfeiffer, Theoretical and experimental investigations of gear-rattling, Nonlinear Dynamics, 2(5) (1991) 367-387.

[2] M.Y. Wang, W. Zhao, R. Manoj, Numerical Modelling and Analysis of Automotive Transmission Rattle, Journal of Vibration and Control, 8(7) (2016) 921-943.

[3] M. Bozca, Torsional vibration model based optimization of gearbox geometric design parameters to reduce rattle noise in an automotive transmission, Mechanism and Machine Theory, 45(11) (2010) 1583-1598.

[4] A. Farshidianfar, A. Saghafi, Global bifurcation and chaos analysis in nonlinear vibration of spur gear systems, Nonlinear Dynamics, 75(4) (2013) 783-806.
[5] L. Xiang, Y. Jia, A. Hu, Bifurcation and chaos analysis for multi-freedom gear-bearing system with time-varying stiffness, Applied Mathematical Modelling, 40 (2016) 10506-10520.
[6] Y. Yi, K. Huang, Y. Xiong, M. Sang, Nonlinear dynamic modelling and analysis for a spur gear system with time-varying pressure angle and gear backlash, Mechanical Systems and Signal Processing, 132 (2019) 18-34.
[7] R. Brancati, E. Rocca, R. Russo, A gear rattle model accounting for oil squeeze between the meshing gear teeth, Proceedings of the Institution of Mechanical Engineers, Part D: Journal of Automobile Engineering, 219(9) (2005) 1075-1083.
[8] R. Brancati, E. Rocca, R. Russo, An analysis of the automotive driveline dynamic behaviour focusing on the influence of the oil squeeze effect on the idle rattle phenomenon, Journal of Sound and Vibration, 303(3-5) (2007) 858-872.
[9] S. Theodossiades, O. Tangasawi, H. Rahnejat, Gear teeth impacts in hydrodynamic conjunctions promoting idle gear rattle, Journal of Sound and Vibration, 303(3-5) (2007) 632-658.
[10] M. De la Cruz, W.W.F. Chong, M. Teodorescu, S. Theodossiades, H. Rahnejat, Transient mixed thermo-elastohydrodynamic lubrication in multi-speed transmissions, Tribology International, 49 (2012) 17-29.
[11] F.H. Liu, S. Theodossiades, L.A. Bergman, A.F. Vakakis, D.M. McFarland, Analytical characterization of damping in gear teeth dynamics under hydrodynamic conditions, Mechanism and Machine Theory, 94 (2015) 141-147.
[12] M. Vaishya, R. Singh, Analysis of Periodically Varying Gear Mesh Systems with Coulomb Friction Using Floquet Theory, Journal of Sound and Vibration, 243(3) (2001) 525-545.
[13] M. Vaishya, R. Singh, Sliding Friction-Induced Non-Linearity and Parametric Effects in Gear Dynamics, Journal of Sound and Vibration, 248(4) (2001) 671-694.
[14] C. Gill-Jeong, Analysis of the nonlinear behavior of gear pairs considering hydrodynamic lubrication and sliding friction, Journal of Mechanical Science and Technology, 23(8) (2010) 2125-2137.
[15] Z. Li, C. Zhu, H. Liu, Z. Gu, Mesh stiffness and nonlinear dynamic response of a spur gear pair considering tribo-dynamic effect, Mechanism and Machine Theory, 153 (2020).
[16] E. Lauster, M. Boos, Heat-balance of mechanical transmission for commercial vehicles, VDI-Berichte, 6(488) (1983) 45-55.
[17] C. Changenet, P. Velex, A Model for the Prediction of Churning Losses in Geared Transmissions—Preliminary Results, Journal of Mechanical Design, 129(1) (2007) 128-133.
[18] C. Gorla, F. Concli, K. Stahl, B.-R. Höhn, K. Michaelis, H. Schultheiß, J.-P. Stemplinger, Hydraulic losses of a gearbox: CFD analysis and experiments, Tribology International, 66 (2013) 337-344.
[19] S. Li, Q. Wu, Z. Zhang, Bifurcation and chaos analysis of multistage planetary gear train, Nonlinear Dynamics, 75(1-2) (2013) 217-233.
[20] F. Liu, L. Zhang, H. Jiang, J. Zhang, Nonlinear dynamic analysis of two external excitations for the gear system using an original computational algorithm, Mechanical Systems and Signal Processing, 144 (2020).
[21] C. Weber, The deflection of loaded gears and the effect on their load carrying capacity, Department of Scientific and Industrial Research, Sponsored Research, Germany, Report No.

3, part I, England, (1949).
[22] BS ISO 6336–1:2006. Calculation of load capacity of spur and helical gears -Part 1: Basic principles, introduction and general influence factors.
[23] Z. Chen, W. Zhai, K. Wang, Vibration feature evolution of locomotive with tooth root crack propagation of gear transmission system, Mechanical Systems and Signal Processing, 115 (2019) 29-44.
[24] J. Wang, J. Zhang, Z. Yao, X. Yang, R. Sun, Y. Zhao, Nonlinear characteristics of a multi-degree-of-freedom spur gear system with bending-torsional coupling vibration, Mechanical Systems and Signal Processing, 121 (2019) 810-827.
[25] Z. Cao, Z. Chen, H. Jiang, Nonlinear dynamics of a spur gear pair with force-dependent mesh stiffness, Nonlinear Dynamics, 99(1-22) (2019) 1227-1241.
[26] Z. Chen, J. Ning, K. Wang, W. Zhai, An improved dynamic model of spur gear transmission considering coupling effect between gear neighboring teeth, Nonlinear Dynamics, 106(1) (2021) 339-357.
[27] D. Guo, F. Chen, J. Liu, X. Shi, D. Luo, Theoretical and Experimental Study of Oil Churning Resistance Torque of High-speed Gear Pair, Journal of Mechanical Engineering, 57(1) (2021) 49-60.
[28] D. Guo, Y. Zhou, Y. Zhou, Y. Wang, F. Chen, X. Shi, Numerical and experimental study of gear rattle based on a refined dynamic model, Applied Acoustics, 185 (2022).
[29] T.A. S., Hydraulic losses in gearboxes with oil immersion, Russian Engineering Journal, 55 (1975) 7-11.
[30] B.R.S. Darrell R , Paul P, Characterizing the Onset of Manual Transmission Gear Rattle Part II Analytical Results, Sae International Journal of Passenger Cars Mechanical Systems, 2(1) (2009) 1365-1376.
[31] R. Gohar, Elastohydrodynamics, 2nd ed., Imperial College Press (2001).
[32] A. Fernandez-del-Rincon, A. Diez-Ibarbia, M. Iglesias, F. Viadero, Gear rattle dynamics: Lubricant force formulation analysis on stationary conditions, Mechanism and Machine Theory, 142 (2019).
[33] Y. Bile, A. Gondhalekar, M. Kumbhar, Studies on Neutral Gear Rattle in Early Stage Design, SAE Technical Papers Series, 1 (2013).